J. Fluid Mech. (2010), *vol.* 653, *pp.* 489–518.
doi:10.1017/S0022112010000431

Rheology of a dilute two-dimensional suspension of vesicles

GIOVANNI GHIGLIOTTI[1], THIERRY BIBEN[2] AND CHAOUQI MISBAH[1]†

[1]Laboratoire de Spectrométrie Physique, UMR 5588, 140 Avenue de la Physique, Université Joseph Fourier Grenoble I, and CNRS, 38402 Saint Martin d'Hères, France

[2]Université de Lyon, Laboratoire PMCN, Université Claude Bernard-Lyon I et CNRS, 43 bvd du 11 Novembre 1918, 69622 Villeurbanne, France

(Received 3 April 2009; revised 21 January 2010; accepted 22 January 2010; first published online 22 April 2010)

The rheology of a dilute two-dimensional suspension of vesicles (closed bags of a lipid bilayer membrane) is studied by numerical simulations. The numerical methods used are based on the boundary integral formulation (Green's function technique) and the phase field approach, which has become a quite popular and powerful tool for the numerical study of free-boundary problems. The imposed flow is an unbounded linear shear. The goal of the present study is to elucidate the link between the rheology of vesicle suspensions and the microscopic dynamics of the constituent particles (tank-treading and tumbling motions). A comparison with emulsion rheology reveals the central role played by the membrane. In particular, at low viscosity ratio λ (defined as the viscosity of the internal fluid over that of the ambient one), the effective viscosity decreases with λ, while the opposite trend is exhibited by emulsions, according to the classical Taylor result. This fact is explained by considering the velocity field of the ambient fluid. The area-incompressibility of the vesicle membrane modifies the surrounding velocity field in a quite different manner than what a drop does. The overall numerical results in two dimensions are in reasonable agreement with the three-dimensional analytical theory derived recently in the small deformation limit (quasi-spherical shapes). The finding that the simulations in two dimensions capture the essential features of the three-dimensional rheology opens the way for extensive and large-scale simulations for semi-dilute and concentrated vesicle suspensions. We discuss some peculiar effects exhibited by the instantaneous viscosity in the tumbling regime of vesicles. Finally, the rheology is found to be relatively insensitive to shear rate.

1. Introduction

A vesicle is a liquid drop enclosed by a phospholipid bilayer and suspended in an aqueous solution. Vesicles are believed to represent an interesting model system for studying the viscoelastic properties of real cells, such as red blood cells (Abkarian & Viallat 2008; Edidin 2003). The dynamics and the rheology of vesicles are a very active field of research nowadays, as evidenced by the large number of recent investigations: (i) numerical (Kaoui, Biros & Misbah 2009; Maitre *et al.* 2009; McWhirter, Noguchi & Gompper 2009; Veerapaneni *et al.* 2009), (ii) analytical (Danker, Verdier & Misbah

† Email address for correspondence: chaouqi.misbah@ujf-grenoble.fr

2008; Finken *et al.* 2008; Lebedev, Turitsyn & Vergeles 2008; Danker, Vlahovska & Misbah 2009) and (iii) experimental (Coupier *et al.* 2008; Kantsler, Segre & Steinberg 2008; Vitkova *et al.* 2008; Deschamps, Kantsler & Steinberg 2009).

While the dynamics of an isolated vesicle has received a lot of attention, vesicle suspensions have been studied to a limited extent. This paper focuses on the flow of a suspension of vesicles where both the internal and the suspending fluids are considered to be Newtonian. The phospholipid molecules are free to move within the membrane, so that the membrane has a two-dimensional liquid-like character. Like a three-dimensional liquid, the membrane is subject to local incompressibility, i.e. constant surface density. This reflects the optimal packing of lipids that balances electrostatic repulsion and hydrophobic attraction between lipid molecules. In addition, the membrane possesses a resistance to bending.

The presence of the membrane has already exhibited its importance in differentiating the dynamics of a vesicle from that of a simple drop (see Keller & Skalak 1982; Kraus *et al.* 1996; Beaucourt *et al.* 2004*b*; Kantsler & Steinberg 2005; Noguchi & Gompper 2005; Misbah 2006; Mader *et al.* 2006). Under shear flow a vesicle exhibits various motions, such as (i) tank-treading (TT), in which the vesicle keeps a fixed orientation with respect to the imposed flow direction while its (fluid) membrane undergoes a tank-treading-like motion, (ii) tumbling (TB), in which the vesicle rotates periodically in the shear plane, and (iii) a vacillating–breathing (or trembling, swinging), which has been predicted by Misbah (2006) and experimentally observed by Kantsler & Steinberg (2006): the vesicle's main axis oscillates about the flow direction, while the shape undergoes a breathing motion. The transition from one regime to another is triggered by changing, for example, the viscosity ratio (ratio of the internal viscosity over that of the suspending fluid). In contrast, a drop (at small enough shear rates so that the drop maintains its integrity) always assumes a stationary shape. The rheology of a dilute suspension of vesicles has been studied recently analytically (see Misbah 2006; Danker & Misbah 2007; Danker *et al.* 2007; Vlahovska & Gracia 2007) and experimentally (see Kantsler *et al.* 2008; Vitkova *et al.* 2008). Analytical theories are based on the assumption that the vesicle shape is close to a sphere. How would a significant deviation from a sphere affect the results is an open question. A red blood cell, for example, has, at equilibrium, a quite pronounced biconcave shape. The large deviation from a sphere makes the extension of the analytical theory quite difficult. Numerical simulations are a tool that allows the analysis of more complex geometries and concentrated suspensions.

In order to extract quantitative dynamical and rheological data from numerical simulations, attention has to be paid to time and space discretization to ensure the convergence of the results. It turns out that the constraint of local area conservation, crucial for vesicles, is very demanding and imposes the use of fine meshes and small time steps. Allowing more than few percents of local area changes gives rise to spurious dynamics, such as vacillating.

As a consequence of the area constraint, three-dimensional simulations are quite time-consuming. Hence, as a first step we limit our study to the case of a two-dimensional suspension. The simplicity of the two-dimensional model allows for a clearer interpretation of the results, as compared to three dimensions. Two-dimensional simulations exhibit similar types of behaviours as those predicted analytically in three dimensions in the dilute regime (see Misbah 2006; Danker & Misbah 2007; Danker *et al.* 2007).

The major point presented here is the clear link between the microscopic dynamics of a vesicle and the overall rheology. In addition, we shall discuss in detail the main

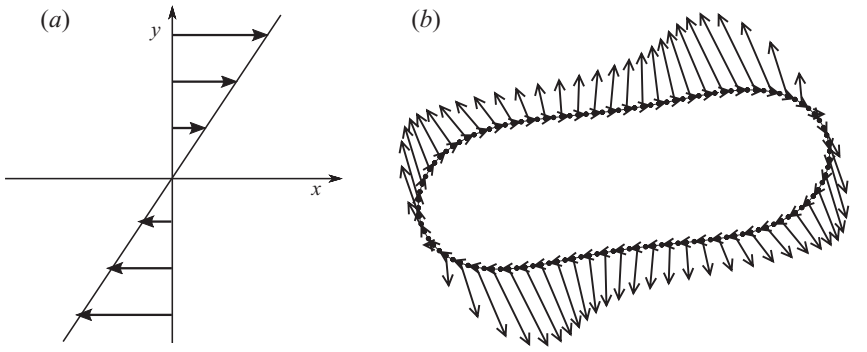

FIGURE 1. (*a*) The imposed linear shear flow and the coordinate system. (*b*) A tank-treading vesicle in linear shear flow with a reduced area of $\alpha = 0.7$, a viscosity ratio of $\lambda = 3$ and a capillary number $C_a = 1$. The dots represent a typical mesh (only half of the grid points are shown), the tangential arrows represent the velocity field and the outward arrows represent the force exerted by the fluid on the membrane.

differences between the behaviour of the effective viscosity for emulsions and vesicle suspensions.

Numerical simulations are carried out by using two different methods: the boundary integral (BI) method, which is based on the use of the Green's function techniques, and the phase field (PF) method. The former is nowadays a reliable standard for simulations of deformable suspended entities, while the latter, although less precise, is more flexible, requires less procedures to pass from a physical system to another (like handling several suspended entities) and is applicable to more general situations, i.e. when the basic fluid equations are not linear (e.g. non-Newtonian ambient fluids). The use of both techniques allowed us to gain a deep insight into this problem and thus to draw robust conclusions.

The paper is organized as follows. Section 2 describes the physical system, § 3 discusses the numerical methods and § 4 presents the results for rheology of a dilute vesicle suspension and compares them with emulsion rheology explaining the differences.

2. The physical system

Since our main goal is to build a basic understanding of the fundamental phenomena linking rheology to microscopic dynamics, we make the following simplifications. We devote this study to the simplest situation: a single two-dimensional vesicle immersed in an unbounded linear shear flow (see figure 1). Starting from the isolated vesicle problem, we are able to extrapolate the results to dilute suspensions, i.e. to a finite concentration, albeit neglecting hydrodynamical interactions.

Most of the available experimental data on vesicles concern the low-Reynolds-number limit (typically of the order of 10^{-3}), so inertia can be neglected. It must be remarked that while the use of the BI method requires linearity of fluid equations, the PF method does not, and hence it can be used in the finite Reynolds number case, if need be.

In the vanishingly small Reynolds number limit, the fluid motion inside and outside the vesicle is described by the Stokes equations

$$-\nabla p + \eta_i \Delta \boldsymbol{u} = 0 \qquad \nabla \cdot \boldsymbol{u} = 0 \tag{2.1}$$

where η_i, with $i = 0, 1$, is the viscosity of the external (0) or the internal (1) fluid. The membrane, subject to the constraint of local incompressibility, is considered in two dimensions as an inextensible and impermeable line endowed with bending resistance. In addition, we apply no-slip boundary conditions between the membrane and both fluids, which leads to a velocity field that is continuous everywhere in the considered domain. The membrane forces are discussed in detail in § 3.1.

The vesicle dynamics is entirely described by three dimensionless parameters (α, C_a, λ) (see Beaucourt, Biben & Misbah 2004*a*). The reduced area is defined as

$$\alpha = \frac{A}{\pi[p/2\pi]^2}, \tag{2.2}$$

where A is the vesicle area (volume in three dimensions) and p is the vesicle perimeter. Also, $\alpha = 1$ for a circle, and $\alpha < 1$ otherwise. Experimentally, the variation of α may be achieved by osmosis: addition of sugar, for example, in the suspending solution causes deflation of the vesicle (loss of water from inside the vesicle towards outside). We introduce a capillary number

$$C_a = \frac{\tau_c}{\tau_u} = \frac{\eta_0 \dot{\gamma} r_0^3}{\kappa}, \tag{2.3}$$

where $\tau_c = \eta_0 r_0^3/\kappa$ is the curvature relaxation time scale, $\tau_u = \dot{\gamma}^{-1}$ is the flow time scale, η_0 is the viscosity of the suspending Newtonian fluid, $\dot{\gamma}$ is the imposed shear rate, κ is the bending modulus of the membrane (see Helfrich 1973) and r_0 is the radius of the equivalent circle (i.e. the radius of a circle having the same area as the vesicle). C_a compares the strength of the imposed flow to the bending resistance of the membrane.

Finally, a third dimensionless number enters the model equations, namely the viscosity ratio

$$\lambda = \frac{\eta_1}{\eta_0}, \tag{2.4}$$

which is the ratio between the viscosities of the internal and external fluids.

The rheological quantities of interest are the effective (shear) viscosity of the solution

$$\eta \equiv \frac{\langle \sigma_{xy} \rangle}{\dot{\gamma}} \tag{2.5}$$

and the normal stress difference

$$N \equiv \frac{\langle \sigma_{xx} \rangle - \langle \sigma_{yy} \rangle}{\dot{\gamma}}, \tag{2.6}$$

where $\boldsymbol{\sigma}$ is the stress tensor of the suspension – which depends on the still-unknown vesicle conformation – and the angle bracket $\langle\ \rangle$ denotes volume average. Note that vesicles are sufficiently large to neglect Brownian motion; the typical vesicle radius is of the order of 10 μm).

It is convenient to subtract the contribution of the imposed flow and normalize the result by an appropriate factor, which includes the volume fraction ϕ of the suspended entities, following Batchelor (1970). The imposed linear shear flow trivially yields $\langle \sigma_{xy} \rangle = \eta_0 \dot{\gamma}$ and $N = 0$, so we have the non-dimensional reduced quantities:

$$[\eta] \equiv \frac{\langle \sigma_{xy} \rangle - \eta_0 \dot{\gamma}}{\eta_0 \dot{\gamma} \phi} \tag{2.7}$$

and

$$[N] \equiv \frac{\langle \sigma_{xx} \rangle - \langle \sigma_{yy} \rangle}{\eta_0 \dot{\gamma} \phi}, \tag{2.8}$$

which will be called the reduced viscosity and reduced normal stress difference, respectively.

The vesicle contribution to the suspension stress is linear in the volume fraction, which expresses the fact that the effects of the vesicles sum up linearly in the absence of hydrodynamic interaction. This kind of approach is expected to provide quantitative results for small enough concentrations (typically $\leqslant 5\,\%$, in reference to the experimental validity of Einstein's result for a suspension of spherical rigid particles, see Larson 1999), since, otherwise, we expect that the hydrodynamic interactions can no longer be neglected.

3. The numerical methods

We use two different numerical methods to run simulations of vesicles immersed in an external fluid: the BI and PF methods. We briefly describe both of them in the following paragraphs.

3.1. *Boundary integral method*

The main idea of this method is to solve Stokes equations by means of the Green's function technique. The use of this method yields the velocity of the membrane, needed for the time evolution of the suspended entities, as a function of integrals over the various boundaries present in the considered fluid domain. For a single vesicle in an unbounded shear flow the only boundary is that of the membrane of the vesicle (see Pozrikidis 1992, 2001). The computation reduces from a two-dimensional problem (fluid domain) to a one-dimensional problem (the vesicle boundary). This is done, however, at a certain price, non-locality: the motion of a given point of the surface of the suspended entity depends on the dynamics of the points that are located elsewhere. The numerical solution of these equations is achieved by a discretization of the vesicle surface, which is a line in two dimensions. Note that this method can only be used to solve linear equations (as Stokes equations) and needs an update of the mesh during the time evolution because of the deformation of the boundaries of the fluid domains (see Rallison & Acrivos 1978; Kraus *et al.* 1996; Cantat & Misbah 1999). Moreover, in two dimensions, the constraint of local length incompressibility on the vesicle membrane preserves the distance between neighbouring points of the discretization, so the mesh update can be performed with a simple Lagrangian advection.

The equation for the velocity of a point belonging to the membrane (denoted by $\boldsymbol{x}_0$ hereafter) is (see Pozrikidis 1993; Kennedy, Pozrikidis & Skalak 1994)

$$\boldsymbol{u}(\boldsymbol{x}_0) = \frac{2}{1+\lambda}\boldsymbol{u}^{\infty}(\boldsymbol{x}_0) + \frac{1}{2\pi\eta_0(1+\lambda)} \oint_{\gamma} \boldsymbol{G}(\boldsymbol{x}-\boldsymbol{x}_0)\cdot\boldsymbol{f}(\boldsymbol{x})\,\mathrm{d}s(\boldsymbol{x}) + \frac{2(1-\lambda)}{\pi(1+\lambda)} \oint_{\gamma} \boldsymbol{u}(\boldsymbol{x})\cdot\boldsymbol{T}(\boldsymbol{x}-\boldsymbol{x}_0)\cdot\boldsymbol{n}(\boldsymbol{x})\,\mathrm{d}s(\boldsymbol{x}), \tag{3.1}$$

where

$$G_{ij}(\boldsymbol{x}-\boldsymbol{x}_0) = -\delta_{ij}\ln|\boldsymbol{x}-\boldsymbol{x}_0| + \frac{(\boldsymbol{x}-\boldsymbol{x}_0)_i(\boldsymbol{x}-\boldsymbol{x}_0)_j}{|\boldsymbol{x}-\boldsymbol{x}_0|^2}, \tag{3.2}$$

$$T_{ijk}(\boldsymbol{x}-\boldsymbol{x}_0) = -4\frac{(\boldsymbol{x}-\boldsymbol{x}_0)_i(\boldsymbol{x}-\boldsymbol{x}_0)_j(\boldsymbol{x}-\boldsymbol{x}_0)_k}{|\boldsymbol{x}-\boldsymbol{x}_0|^4} \tag{3.3}$$

are the Green's functions of the problem (G_{ij} refers to the so-called single-layer contribution, while T_{ijk} accounts for the double-layer contribution), $\boldsymbol{u}^{\infty}$ represents the imposed flow, γ is the vesicle contour and $\boldsymbol{f}$ is the membrane force, given by

$$\boldsymbol{f} = -\kappa \left[\frac{\mathrm{d}^2 c}{\mathrm{d}s^2} + \frac{1}{2} c^3 \right] \boldsymbol{n} + \zeta c \boldsymbol{n} + \frac{\mathrm{d}\zeta}{\mathrm{d}s} \boldsymbol{t}. \tag{3.4}$$

This force is obtained from the functional derivative of the Helfrich bending energy (Canham 1970; Helfrich 1973) including the local arclength constraint (expressing inextensibility). The bending energy, together with the contribution due to membrane incompressibility, has (in two dimensions) the form

$$E = \frac{\kappa}{2} \oint_{\gamma} c^2 \mathrm{d}s + \oint_{\gamma} \zeta \mathrm{d}s, \tag{3.5}$$

where s represents the curvilinear coordinate on the contour of the vesicle, c is the local curvature of the membrane and $\boldsymbol{n}$ and $\boldsymbol{t}$ are the outward normal and the tangent vectors. Also, ζ is a local Lagrange multiplier associated with the constraint of local surface (length in two dimensions) inextensibility. The expression of the membrane force has been used in Cantat (1999), and a simple derivation can be found in the Appendix of Kaoui *et al.* (2008).

For numerical reasons, the numerical scheme that is implemented in the code does not use ζ directly, but rather a tension-like parameter, introduced as a penalty:

$$\boldsymbol{f} = -\kappa \left[\frac{\mathrm{d}^2 c}{\mathrm{d}s^2} + \frac{1}{2} c^3 \right] \boldsymbol{n} + T \left[(\ell_l - \ell_{l_0}) \boldsymbol{\tau}_l + (\ell_r - \ell_{r_0}) \boldsymbol{\tau}_r \right], \tag{3.6}$$

where $(\ell_l - \ell_{l_0})$ and $(\ell_r - \ell_{r_0})$ are the differences between the actual distances of a discretization point of the membrane to its left and right neighbours and their initial values. Likewise, $\boldsymbol{\tau}_l$ and $\boldsymbol{\tau}_r$ are the unit vectors pointing from the considered point to the corresponding neighbours. This tension term accounts for both the tangential and normal components of the membrane incompressibility force that enters via the Lagrange multiplier ζ in (3.4). We can introduce a dimensionless number associated with T and defined as $C_T = \eta_0 \dot{\gamma}/(r_0 T)$. The elastic constant T is taken quite large, so that the corresponding force is large enough to fulfil quasi-conservation of the local length at the time scale imposed by the action of physical forces. This means that the elastic dynamics can be considered as an effective implementation of quasi-instantaneous local membrane incompressibility (see Cantat, Kassner & Misbah 2003) (in practice, taking $T \approx 10^4$, when the other relevant parameters are of order 1, is already sufficient to reach the convergence of this scheme). More precisely, if C_a is of order 1, then C_T should be chosen small enough (typically 10^{-4} or smaller).

Because of the large separation of time scales, the time step has to be sufficiently small to resolve local dynamics that occur on time scales much shorter than the mesoscopic dynamics of the whole vesicle. An advantage of the use of the penalization method is that we do not need to solve numerically for a Lagrange multiplier, which should be obtained implicitly from the condition that the surface divergence of the velocity field must vanish.

The membrane velocity is computed by evaluating the right-hand side of (3.1): we prescribe an initial vesicle shape as well as an initial velocity on the membrane, so that the right-hand side of (3.1) can be evaluated at initial time. Then time integration is carried out by means of an explicit Euler scheme, in which the velocity appearing

on the right-hand side of (3.1) is taken to be the one computed at the previous time step. Each point on the membrane is displaced by a quantity $\boldsymbol{u}\Delta t$, where Δt is the time step and $\boldsymbol{u}$ is the membrane velocity, and this yields the new configuration, and so on.

The rheological properties are computed following Batchelor's approach (see Batchelor 1970), adapted to liquid particles as in Kennedy *et al.* (1994):

$$\langle \sigma_{ij} \rangle = \frac{1}{S}\left[\eta_0 \int_S (\partial_i u_j + \partial_j u_i)\, \mathrm{d}A + \oint_\gamma [x_j f_i + \eta_0(\lambda - 1)(n_i u_j + n_j u_i)]\, \mathrm{d}s\right], \qquad (3.7)$$

where S denotes the bulk of the system and γ denotes the contour of the vesicle. The first term, which is the average velocity gradient in the system, represents the stress contribution of the imposed flow (see Schowalter, Chaffey & Brenner 1968; Batchelor 1970; Frankel & Acrivos 1970), while the second term accounts for the presence of the vesicle. We shall thus focus on the latter contribution.

3.1.1. *Numerical implementation and convergence test*

BI method is very accurate and thus allows for precise quantitative results. We have studied the numerical convergence of the code upon decreasing the time step and increasing the number of discretization points. The method of discretization is described by Cantat *et al.* (2003). It turned out that the convergence with respect to the time step is quite fast, while the convergence with respect to the spatial discretization n is slower: we focused then our attention on the latter. We ran four series of simulations, with $n \in \{60, 80, 120, 240\}$. For every series we chose a time step for which we can consider that the time convergence is attained: (simulations with a time step three times smaller were giving the same results within an error of 10^{-5}). For this convergence test we consider a vesicle with a reduced area $\alpha = 0.9$ and a capillary number $C_a = 1$.

We have analysed the behaviour of the critical viscosity ratio λ_c beyond which the vesicle undergoes a tumbling transition. It is in general quite difficult to locate with a good enough accuracy a bifurcation point. The results are shown in figure 2. The same quantity is also computed for $n = 480$ (in that case we only focus on the critical value λ_c, in which we do not compute the whole curves as in figure 2 because of the rather large computing time). In figure 3, we report λ_c for different values of n. In order to check the convergence by extrapolation to $n = \infty$, we plot λ_c as a function of $1/n$. It is appealing to fit the data with a parabola (see figure 3). Taking a test function $y = ax^2 + d$ (we have omitted the linear term since the figure conveys the impression of a quite small slope at the origin) it is found that the discrepancy between the extrapolated value at $n \to \infty$ ($d = 5.50$) and the one found by the most refined simulation ran ($n = 240$, $\lambda_c = 5.55$) is about 1 %: so we can consider that our discretization is close enough to convergence to be able to discuss the results at a quantitative level. The time step for $n = 240$ is $\Delta t = 3 \times 10^{-5}$. CPU time on a desktop processor is of the order of hours or days – depending on the parameter values. The perimeter is conserved within a relative error of 10^{-3}, and the surface of 10^{-6}.

3.2. *Phase field method*

This technique is traced back to van der Waals (see van der Waals 1979) and has been widely used in the context of critical phenomena (see Hohenberg & Halperin 1977). The method has then been used for non-equilibrium pattern-forming solidification problems (see Penrose & Fife 1990; Kobayashi 1993; Wheeler,

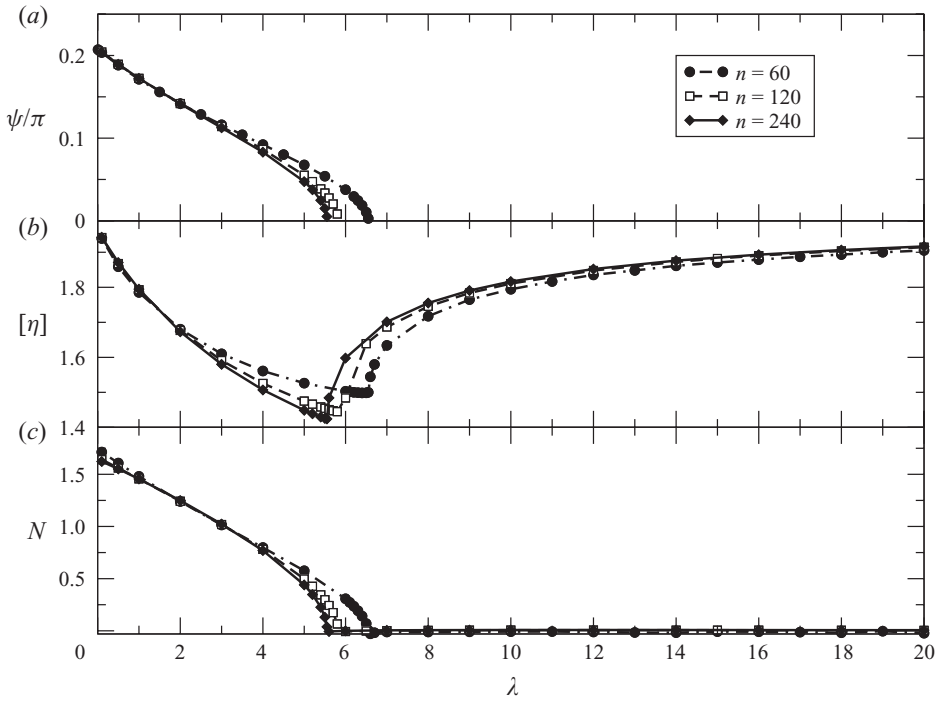

FIGURE 2. Boundary integral method: numerical convergence upon increasing n. (a) Stationary inclination angle ψ, measured counterclockwise from the positive x semi-axis (when a stationary solution exists; this is the tank-treading regime), (b) the reduced viscosity $[\eta]$, and (c) the normal stress difference N as a function of the viscosity ratio λ. The reduced area is $\alpha = 0.9$ and the capillary number $C_a = 1.0$. Rheological measurements of (b) and (c) have been averaged over a period in the tumbling regime.

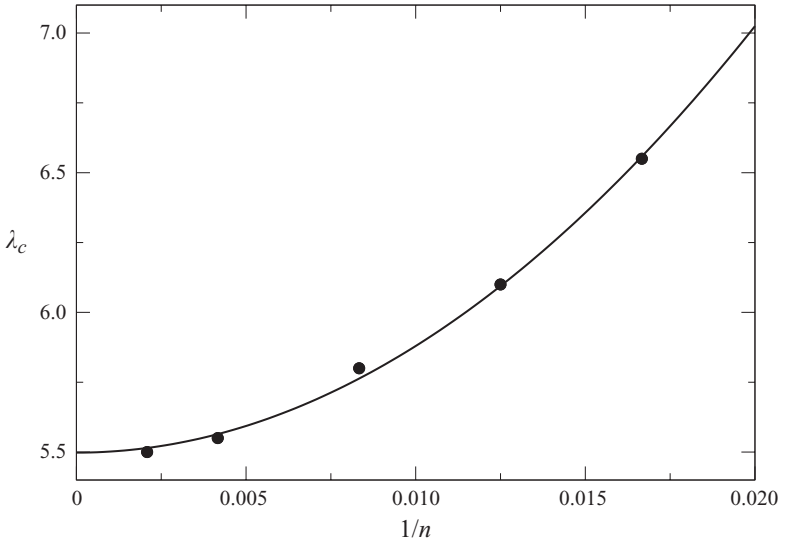

FIGURE 3. Boundary integral method: numerical convergence of the parameter λ_c as a function of $1/n$. Here $n \in \{60, 80, 120, 240, 480\}$. The line represents the fit of the results by the function $y = ax^2 + d$. The value found for the intersection with the y axis is $d = 5.50$, representing the extrapolation for $n \to \infty$.

Boettinger & McFadden 1993; Wang *et al.* 1993). It was first introduced for vesicles and membranes by Biben & Misbah (2002, 2003) and Biben, Kassner & Misbah (2005). This method is based on the introduction of an auxiliary field, namely the phase field, which assumes two constant values inside and outside the vesicle (in our case -1 and $+1$ respectively), and undergoes a continuous, albeit stiff enough, variation between these values across the membrane position.

Unlike the van der Waals and phase transition problems where the phase field represents a physical quantity (e.g. density), for the vesicle system it can, at first sight, be viewed as a colour-like function that delimits the interior of the vesicle from the exterior. Recently a thermodynamical formulation of the phase field for membrane position has been proposed, although the notion of thermodynamics associated with a membrane position is *a priori* not easy to imagine (see Jamet & Misbah 2007, 2008*a*,*b*). Here we shall adopt the alternative of a colour-like function.

The phase field behaves as a $\tanh(r/\epsilon)$ profile (where r is the position variable across the membrane). We refer thus to the phase field as a diffuse interface model, because the boundary region is endowed with a certain thickness ϵ, which is not of atomic size (otherwise the problem would be too stiff and could not be handled numerically within a reasonable time), but rather it is required to remain small enough in comparison with the vesicle size and the local radius of curvature. Thus, the thickness of the interface is artificial and does not reflect the physical thickness of the bilayer, since here the phase field is used only for interface tracking. This results in some conceptual and numerical difficulties, the most serious one being the need to extrapolate the results in the limit of vanishing interface thickness (see Beaucourt *et al.* 2004*b*). This extrapolation is not always obvious, since the dynamics is sensitive to the value of the interface thickness.

The PF method is a field approach, i.e. the evolution equations are solved everywhere in the bulk regardless of the position of the membrane. The presence of the vesicle in the considered domain is expressed explicitly only in the initial condition. The popularity of the PF approach is due to its various virtues such as (i) the possibility to run simulations for any kind of constitutive equation for the ambient fluid (not only linear as is required by the BI method), (ii) the absence of direct tracking of the interface, thanks to which remeshing problems and others due to singularities over the boundaries are avoided and (iii) simulating several vesicles requires only a change in the initial conditions.

Let us recall the model equations initially reported in Biben & Misbah (2002, 2003). The Stokes equations are coupled with an evolution equation for the phase field φ. The latter is derived from a phenomenological free energy (which has the form of a Ginzburg–Landau energy known for phase transition phenomena) having a double well and a wall-like contribution. In addition, the bending force and the inextensibility condition of the membrane (which is a proper problem to vesicles) have to be defined everywhere in the bulk, like the phase field itself. This is detailed by Beaucourt *et al.* (2004*b*).

The evolution equations of the PF model read:

$$\frac{\partial \boldsymbol{u}}{\partial t} = \nabla \cdot [\eta(\varphi)(\nabla \boldsymbol{u} + \nabla \boldsymbol{u}^{\mathrm{T}})] - \nabla P + \boldsymbol{f}, \tag{3.8}$$

$$\frac{\partial \varphi}{\partial t} = -\boldsymbol{u} \cdot \nabla \varphi + \epsilon_{\varphi} \left[-\frac{\delta F}{\delta \varphi} + c\epsilon^2 |\nabla \varphi| \right], \tag{3.9}$$

$$\frac{\partial \zeta}{\partial t} = -\boldsymbol{u} \cdot \nabla \zeta + T \nabla_s \cdot \boldsymbol{u}, \tag{3.10}$$

where $\boldsymbol{n} = \nabla\varphi/|\nabla\varphi|$ is the normal to the iso-φ lines, $c = -\nabla \cdot \boldsymbol{n}$ is the curvature, $\eta(\varphi) = \eta_0(1+\varphi)/2 + \eta_1(1-\varphi)/2$ is the position-dependent viscosity (this parametrization allows to account for a viscosity contrast between the interior and exterior of the vesicle), P is the pressure, and $\boldsymbol{f}$ represents the force on the membrane,

$$\boldsymbol{f} = \left[-\kappa\left[\frac{c^3}{2} + \nabla_s c\right]\boldsymbol{n} + \zeta c\boldsymbol{n} + (\boldsymbol{t}\cdot\nabla\zeta)\boldsymbol{t}\right]\delta^{interface}(\boldsymbol{r}) \tag{3.11}$$

and

$$F = \int_S \mathrm{d}A\left[\frac{1}{4}(1-\varphi^2)^2 + \frac{\epsilon^2}{2}|\nabla\varphi|^2\right] \tag{3.12}$$

is the free energy functional intrinsic to the phase field model. Note that the membrane force is nothing but expression (3.4) written in the phase field spirit. The term $\delta^{interface}(\boldsymbol{r}) = |\nabla\varphi|/2$ localizes the force action around the membrane of the vesicle (the interface of the PF) and is a diffuse version of the Dirac function. Note that $\nabla_s \cdot \boldsymbol{u}$ is the surface divergence of the velocity field, T is similar to the tension-like parameter introduced in (3.6), and has to be large enough in order to enforce the local incompressibility of the membrane, and finally $\boldsymbol{t}$ denotes the tangent vector to the iso-φ contours.

In (3.9), the term $c\epsilon^2|\nabla\varphi|$ has been added in order to suppress the surface tension effect arising from the Laplacian $\nabla^2\varphi$ (that stems from the functional derivative of $|\nabla\varphi|^2$) in the free energy. In fact this term, being a positive contribution to interface energy, acts to reduce the extent of the interface as a surface tension would do. This trick has been introduced by Folch *et al.* (1999), and adopted later for vesicles by Biben & Misbah (2003). Note that this effect can also be suppressed directly from the energy (see Jamet & Misbah 2008*a*), an advantage that may prove useful when using a weak formulation for solving the equations by means of a finite element technique.

The time evolution is implemented after discretizing the space operators by Fourier transforms (see Biben 2005). This requires periodic boundary conditions. As a consequence, the system simulated is more appropriately an infinite periodic system, with an infinite number of vesicles. To avoid the effect of interaction between the vesicle and its images, we run simulations at a low volume fraction $\phi \approx 2\,\%$, corresponding to a squared box whose side is approximately six times the linear dimension of the vesicle. The discretization domain is a squared grid of size 200×200. The number of points lying in the membrane region (the so-called diffuse interface) is equal roughly to 160.

The effective viscosity, from which the intrinsic viscosity is deduced according to (2.7), is computed by integrating the stress tensor over the sides of the simulation box:

$$\eta = \frac{1}{2L\dot{\gamma}}\int_{\partial S}\sigma_{xy}\,\mathrm{d}l = \frac{1}{2L\dot{\gamma}}\int_{\partial S}\eta_0(\partial_x u_y + \partial_y u_x)\,\mathrm{d}l, \tag{3.13}$$

where ∂S represents the boundary of the simulation box of side L (the two sides parallel to the gradient of the imposed shear flow do not contribute to the result due to periodic boundary conditions). The above contribution contains both the effect of the imposed flow and the induced contribution due to the presence of the vesicle.

3.3. *Comparison between the numerical methods*

The results obtained by the two numerical methods are compared in figure 4. It is seen that the two methods show the same qualitative behaviour. However, the PF method is sensitive to the numerical value of the interface width ϵ, and is expected

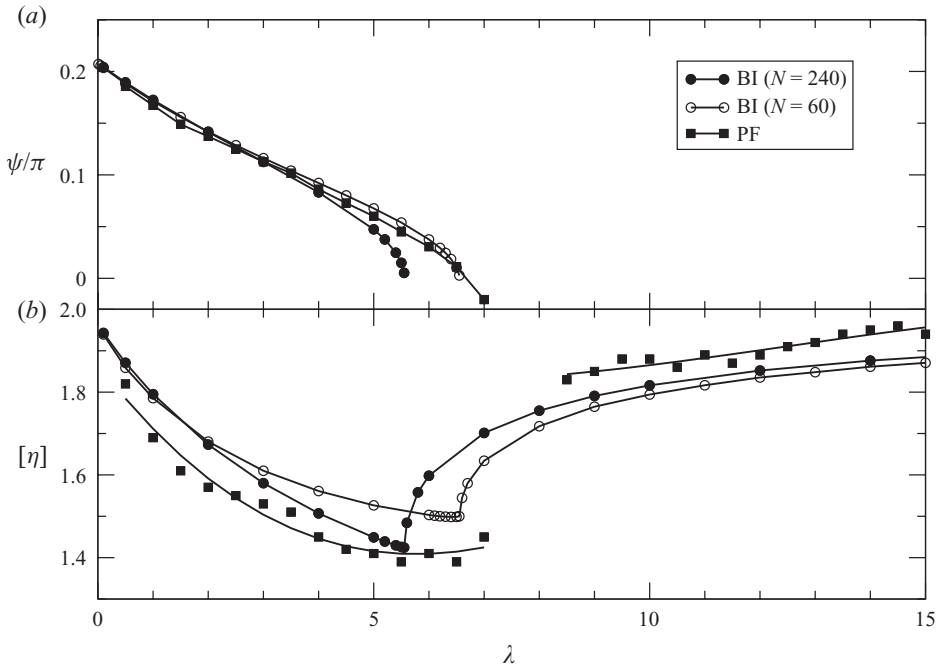

FIGURE 4. Comparison between boundary integral (BI) at two different resolutions, $N = 60$ and $N = 240$, and phase field (PF) results (200×200 grid) extrapolated to $\epsilon \to 0$.

to provide less precise results, unless a very refined mesh is used. If the mesh is not fine enough the PF method shows a significant quantitative deviation from BI results. However, if a larger mesh size is allowed for the BI method, then the BI and PF methods agree even quantitatively, as shown in figure 4. In order to achieve a high enough precision an extrapolation of the PF results to $\epsilon \to 0$ is needed. Because of the extrapolation, this method predicts a slightly negative inclination angle close to the transition; this should be regarded as a numerical artefact. Note, however, that small negative angles are predicted analytically in three dimensions (see Danker *et al.* 2007; Lebedev *et al.* 2008), but no support is known in two dimensions. In addition, the presence of a bifurcation makes the task even more serious numerically, since physical properties undergo an intrinsic rapid change in the vicinity of the bifurcation point. As a consequence, the computation of the effective viscosity (figure 4*b*) in the bifurcation region is hardly accessible, and could not so far have been determined with a high enough degree of confidence.

4. Rheology of a suspension of vesicles

In the dilute regime, the rheological properties of a suspension can be deduced from the dynamics of an isolated vesicle, as shown in § 2. Of particular interest are the reduced viscosity and the reduced normal stress difference. These quantities provide information on the viscous and the non-Newtonian behaviour of the fluid. While the volume fraction of the suspension only plays a trivial role in the dilute regime, the non-trivial control parameters are associated with the dynamics of the vesicle itself: the viscosity ratio, $\lambda \equiv \eta_1/\eta_0$, the capillary number C_a, which expresses the intensity of the flow compared to the bending forces on the membrane, and

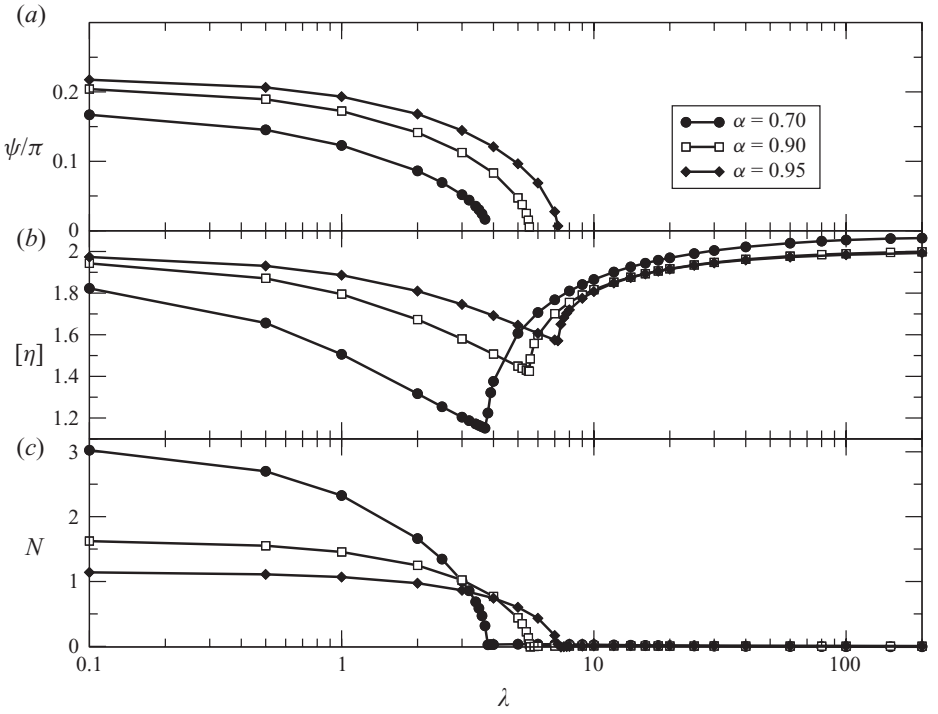

FIGURE 5. Dynamics and rheology of a suspension of vesicles for reduced area $\alpha \in \{0.70, 0.90, 0.95\}$ and a capillary number $C_a = 1.0$. (*a*) The stationary inclination angle ψ (when a stationary solution exists), (*b*) the reduced viscosity $[\eta]$ and (*c*) the normal stress difference N as a function of the viscosity ratio λ.

the reduced area α of the vesicle. Figures 5 and 6 show the steady angle in the tank-treading regime, the reduced viscosity and the reduced normal stress difference. We can see a strong dependence of the reduced viscosity on λ, varied in the interval $[0.1, 200]$. At low λ the vesicle motion is of tank-treading type, while at large λ the vesicle tumbles. The minimal suspension viscosity is obtained at the critical value λ_c corresponding to the bifurcation from tank-treading to tumbling. A detailed discussion of these behaviours is provided in 4.1, while in § 4.2 the normal stress difference is analysed. Although we shall mainly consider the λ dependence, the two other parameters α and C_a are expected to play a role as well. We show in figures 5 and 6 the influence of α, by considering values ranging from $\alpha = 0.70$, quite elongated vesicles, to $\alpha = 0.95$ for nearly circular shapes (see figure 7). We can see that the influence of α is only quantitative, the qualitative behaviour is preserved. Section 4.3 provides a detailed analysis of rheology in the tumbling regime. The influence of C_a will be discussed in § 4.4. In § 4.5 a detailed comparison with drops is drawn. Section 4.6 is devoted to the comparison to three-dimensional results, both analytical and experimental.

Note that these results have been obtained using the BI method for two-dimensional vesicles. As a consequence, in principle, these results have to be compared to two-dimensional theories. An analytical solution for the velocity field in two dimensions has been provided recently by Finken *et al.* (2008). We have used this solution and attempted to derive the effective viscosity. However, the result shows a significant

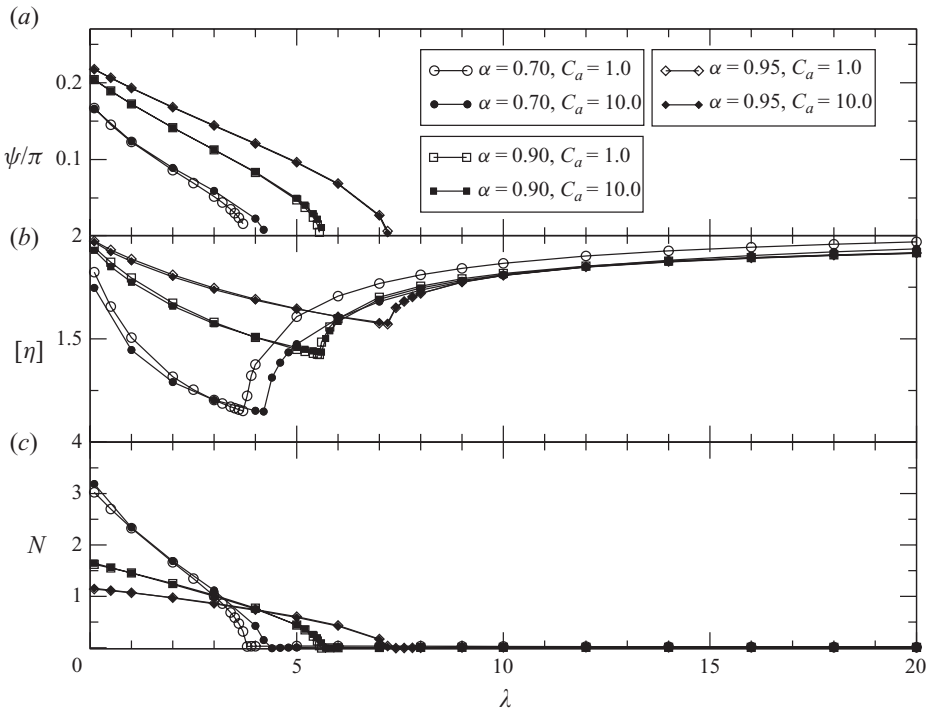

FIGURE 6. Dynamics and rheology of a suspension of vesicles for different reduced areas α and capillary numbers C_a. (*a*) The stationary inclination angle ψ (when a stationary solution exists), (*b*) the reduced viscosity $[\eta]$ and (*c*) the normal stress difference N as a function of the viscosity ratio λ.

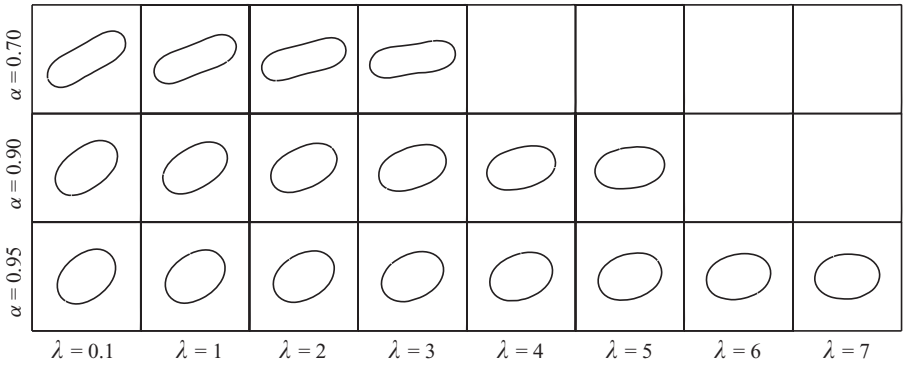

FIGURE 7. Stationary shapes of vesicles for different reduced areas α and a capillary number $C_a = 1.0$. For more elongated vesicles (smaller α) the tumbling to tank-treading transition occurs for smaller values of the viscosity ratio λ.

difference with the expected intrinsic viscosity in the circular limit (which is equal to 2). It is likely that that paper suffers from some typing mistakes.

The reduced suspension viscosity of quasi-circular vesicles ($\alpha = 0.95$) approaches the value 2.0 in the two extreme limits, $\lambda \to 0$ and $\lambda \to \infty$, as shown in figures 5(*b*) and 6(*b*). The three-dimensional analogue approaches the value 2.5 (see Danker & Misbah 2007; Danker *et al.* 2007) for quasi-spherical vesicles. These two values turn out to be

equal to the Einstein coefficients in two and three dimensions, representing the effective viscosity of a dilute suspension of rigid circles or spheres (see Einstein 1906, 1911; Belzons *et al.* 1981; Brady 1984) respectively. The fact that the effective viscosity of rigid particles quantitatively depends on the spatial dimensions is also manifested by a vesicle suspension. This observation allows us to attempt a quantitative comparison between the results of two and three dimensions thanks to a simple rescaling of the data (§ 4.6).

4.1. *The effective viscosity*

The effective viscosity of a suspension of vesicles has a complex behaviour, strongly dependent on the microscopic dynamics. When plotted as a function of the viscosity ratio (figures 5*b* and 6*b*), $[\eta]$ shows a nonlinear and non-monotonic behaviour. We shall first consider the two limiting cases $\lambda \to 0$ (small internal rigidity) and $\lambda \to \infty$ (high internal rigidity). As already pointed out, the intrinsic viscosity approaches the value of the Einstein coefficient in two dimensions, 2.0, in both limits, provided that the shape is quasi circular ($\alpha = 0.95$). For $\lambda \to 0$ this result is not quite surprising. Indeed, at low values of λ the vesicle performs tank-treading motion, and if its shape is close to a circular one ($\alpha = 0.95$) its motion is close to that of a rigid rotation of a circle. The limit $\lambda \to \infty$ is somehow less trivial at first sight. The vesicle undergoes a periodic tumbling motion and thus changes periodically its orientation. However, for a quasi circular shape, a tumbling motion is quite close to a tank-treading motion (a circle is a degenerate limit where tank-treading and tumbling coincide (see Rioual, Biben & Misbah 2004). In conclusion, the fact that $[\eta]$ approaches the value 2 in both limits (large and small λ) seems to have the same origin.

The limiting values of the effective viscosity (i.e. at $\lambda = 0, \infty$) depend on the reduced area α. For $\lambda = 0$ $[\eta]$ decreases upon decreasing α. This effect is not trivial, since the cross-section of the vesicles in the flow, which may be considered as an indicator of flow resistance, does not vary noticeably (actually it even increases slightly, figure 7). The key point to explain this effect is that upon reducing α the vesicle has a more elongated shape, a fact that reduces the deformation of the flow lines, and thus lowers dissipation. At large λ this effect is reversed, figure 5(*b*). That is to say the elongation of vesicles (due to a decrease of α) leads to an increase of $[\eta]$. This means that the disturbance of the flow lines, and hence the effect on dissipation, due to the tumbling vesicle on the imposed velocity field is stronger and stronger. A detailed analysis of the intrinsic viscosity in the tumbling regime is provided in § 4.3.

The same behaviour is obtained analytically in three dimensions: the intrinsic viscosity decreases with Δ, the excess area from a sphere – increasing Δ is equivalent to reducing the reduced volume – in the $\lambda \to 0$ limit (where it lies below the Einstein value), whereas it increases for $\lambda \to \infty$, where $[\eta]$ exceeds slightly the Einstein value (Danker & Misbah 2007; Danker *et al.* 2008).

In the tank-treading regime $[\eta]$ is a decreasing function of λ. The reason is as follows: by increasing λ the inclination angle with respect to the flow decreases, and thus the vesicle opposes less resistance to the flow (see figures 6*a*, *b* and 7). A detailed analysis of this phenomenon is given in § 4.5.

Let us provide further physical explanations to the above results. We have seen that after the transition to tumbling the effective viscosity (averaged over a period) increases with λ (see figure 6*b*). The key ingredient is that, on average, in the tumbling regime the vesicle scans a larger cross-section against the flow, and this results in an enhanced resistance to flow compared to tank-treading. In addition, despite the existence of a bifurcation, $[\eta]$ is continuous at the TT–TB point and exhibits a

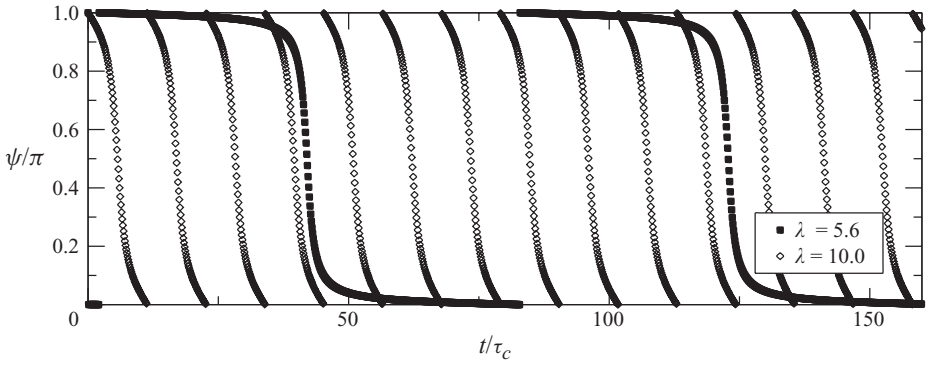

FIGURE 8. Inclination angle as a function of time for vesicles with different λ. $\alpha = 0.90$, $C_a = 1.0$.

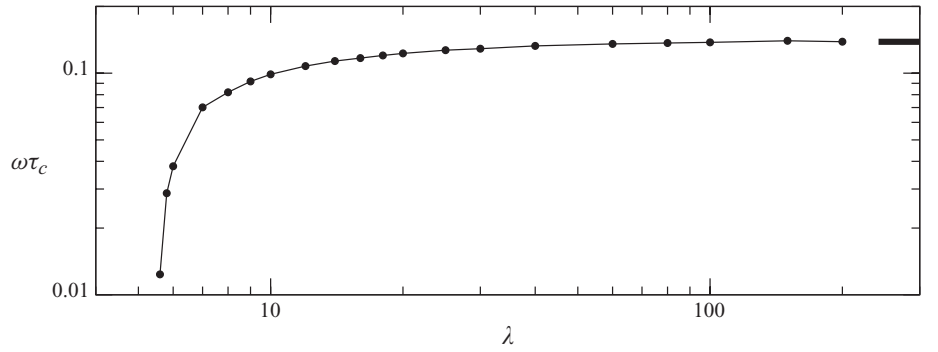

FIGURE 9. Tumbling frequency ω for vesicles with $\alpha = 0.9$ and $C_a = 1.0$ as a function of λ. The results (obtained from BI) have been extrapolated to the limit $n \to \infty$. The thick horizontal segment on the extreme right represents the TB frequency for a rigid ellipse having the same α.

minimum. The vesicle spends, close to the transition point, and on the TB side, most of its time aligned with the flow, and makes a rotation by an angle close to π in a small time interval. This is visible in figure 8 where we show the inclination angle as a function of time with parameters chosen both close to the tumbling bifurcation point ($\lambda = 5.60$, $\lambda_c = 5.55$) and far away from this point ($\lambda = 10.0$). The continuous decrease of the relative time spent in the flow-aligned position is the main reason why $[\eta]$ increases continuously upon increasing λ in the vicinity of the bifurcation point, i.e. for $\lambda \simeq \lambda_c$. As λ increases beyond λ_c, the TB frequency increases towards the value of a rigid ellipse (figure 9), which can be computed analytically (see Keller & Skalak 1982):

$$\omega_R = \frac{\dot{\gamma}}{\pi}\left(\frac{a}{b} + \frac{b}{a}\right)^{-1}, \tag{4.1}$$

where a and b are the lengths of the small and large axes of the ellipse. For an ellipse with a reduced area $\alpha = 0.90$ and for a shear rate $\dot{\gamma} = 1.0$ we have $\omega \cong 0.138$, which is very close to the value found here for a nearly rigid ($\lambda = 200$) vesicle with the same reduced area $\alpha = 0.90$ and at a capillary number $C_a = 1.0$ (see figure 9).

More recently, an analytical expression for the reduced viscosity in three dimensions in the TB regime has been reported (see Vitkova *et al.* 2008). This expression is valid at small enough C_a where the assumption of a shape-preserving solution is expected to

make sense. The analytical expression agrees qualitatively well with the full numerical calculation (figures 6 and 20), in that it shows a square root singularity at the TT–TB point (on the TB side). To be more precise, a fit of the reduced viscosity in the tumbling regime close to the transition with the function $[\eta] = \eta_c + a(\lambda - \lambda_c)^b$ gives an exponent $b \approx 0.4$, which, although slightly different from the theoretical prediction in three dimensions (it is 0.5), is still consistent with a vertical tangent for $\lambda = \lambda_c$.

Note that some features of the three-dimensional analytical work are not captured by the present simulations, however. Indeed, in three dimensions the cusp singularity exhibited by $[\eta]$ at low enough C_a is smeared out at large enough C_a (see Danker *et al.* 2007). In contrast, in the present simulation the cusp is preserved even at high enough C_a. We believe that this behaviour is linked with the fact that in three dimensions a third dynamical regime, called vacillating-breathing (or swinging) is observed (see Kantsler & Steinberg 2006; Misbah 2006; Danker *et al.* 2007), while in the two-dimensional case there is no support to its existence, at least as long as thermal fluctuations are not taken into account; see Messlinger *et al.* (2009). As a consequence, the inclination angle does not show a square root singularity at the tumbling threshold, in contrast with the present two-dimensional simulations where this singularity survives. We believe that the cusp exhibited by $[\eta]$ is directly linked with the behaviour of the inclination angle.

The first conclusion that can be drawn is that, besides the VB mode, the dynamics and rheology of a vesicle in two dimensions are qualitatively similar to their three-dimensional analogues. The presence of the VB mode in three dimensions suppresses the cusp singularity in the behaviour of the effective viscosity at large enough C_a but does not affect the overall qualitative behaviour. These results support the fact that two-dimensional simulations are capable of capturing several essential physical properties. When these simulations fail to explain a given feature found in three dimensions (the only situation encountered so far is the suppression of the cusp singularity) it has even been possible to provide a basic reason, and thus to provide to the two-dimensional work a robust status.

4.2. *The normal stress difference*

We have analysed the behaviour of the normal stress difference N, and linked it to the vesicle dynamics (figure 6). N decreases during tank-treading upon increasing the viscosity ratio. At the critical point N vanishes and remains zero in the tumbling regime (figure 5*c*).

This behaviour of the normal stress difference is more difficult to interpret than the effective viscosity. Here again, the incompressibility of the membrane is an essential ingredient, but it enters in a quite subtle way.

In fact, the direct effect of the incompressibility of the membrane is the generation of a tangential force. The curvature of the membrane introduces a normal component too, as can be seen in (3.4). The normal force is a combination of bending rigidity and the Lagrange multiplier ζ. Actually, the main source giving rise to normal stress difference comes from ζ. This can be shown by analysing the force field over the membrane. In fact, in a flow that is antisymmetric (with respect to the centre), the inextensibility force, which is a response to the flow action, has to be antisymmetric too. This antisymmetry is exhibited by the total force field on the membrane represented in figure 1, showing that the tension component dominates over the bending one (which is symmetric). If we apply (3.7) for the normal components σ_{xx} and σ_{yy}, we see that the (antisymmetric) force is multiplied by the (trivially antisymmetric) position vector, thus giving symmetric contributions that do not then cancel out when integrated over

the membrane of the vesicle. Thus, a non-zero normal stress difference is compatible with the symmetry of the problem in the stationary tank-treading regime.

The normal stress difference drops to zero when the vesicle is at the transition between tumbling and tank-treading (at the transition a tank-treading vesicle has its main axis parallel to the flow). This is due to the additional mirror symmetry: the vesicle exhibits, at the critical point, an up-down symmetry as well as rear-front symmetry, resulting in a vanishing normal stress difference.

4.3. *Instantaneous stress in the tumbling regime*

In the previous sections when referring to vesicles in the tumbling regime we have only presented rheological quantities that have been averaged over a period. We would like to analyse the time dependence of stress, from which we may extract the analogues of effective viscosity (that may be called instantaneous viscosity) and normal stress difference. It must be stressed that, from a theoretical point of view, the way this quantity is defined is similar to the classical definition of the effective viscosity, by using the Batchelor formula (3.7). Thus this definition is not ambiguous, and can be called instantaneous viscosity. Of course, one has to keep in mind that in traditional rheological experiments only an average over time would make sense, due to the uncorrelated dynamics of the vesicles (in the dilute regime) in the sample. Nevertheless, measuring the instantaneous variation of the stress tensor due to a single vesicle can be performed without ambiguity. Moreover, the notion of instantaneous stress is not only of a fundamental interest but is also experimentally measurable with the advent of microfluidic devices and nanoelectromechanical systems (NEMS). These devices are nowadays capable of measurements with high time resolution on fluid samples with a volume smaller than a microlitre (see Boskovic *et al.* 2002; Willenbacher & Oelschlaeger 2007). Sensing the disturbance of the stress by the presence of a vesicle seems to lie within the precision of experiments. However, the measure would not necessarily reflect the value of an average stress, since the probe sees the medium as a continuum. Nonetheless, the presence of a vesicle will disturb the medium, and should have an affect. This question should deserve an analysis under close scrutiny in the future. Our main objective is basically to draw attention to the fact that measurement on such small scales may become quite feasible in the near future. The question addressed here may help triggering future experimental research along this direction.

Figure 10 shows snapshots of a tumbling vesicle and figure 11 shows the time dependence of its inclination angle, reduced viscosity and normal stress difference. The capillary number is set at $C_a = 1.0$, but note that all the features discussed in the following are also exhibited at $C_a = 10.0$. The behaviour of both effective viscosity and normal stress difference is highly nonlinear and exhibits maxima and minima. This feature, found here numerically, was also briefly reported analytically in three dimensions (see Danker & Misbah 2007). A surprising feature is that the effective viscosity exhibits two minima within each tumbling period. A convenient representation that lends itself to a simple interpretation of the results is to plot these quantities as functions of the inclination angle, rather than time, as shown in figure 12. Note that the vesicle orientation is defined modulo π (and not 2π), owing to central symmetry. Here we see clearly that the two maxima of dissipation occur at the inclination of $\pm\pi/4$. Let us recall that a linear shear flow can be written as a superposition of pure rotational and elongational components; elongation is oriented at $\pm\pi/4$ (see Rioual, Biben & Misbah 2004) with respect to the imposed flow direction, as sketched in figure 13. Only the elongational component (that

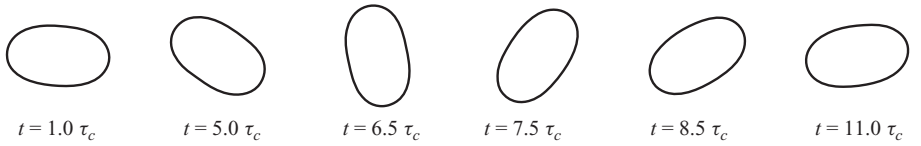

FIGURE 10. Tumbling of a vesicle in a linear shear flow. $\lambda = 8$, $\alpha = 0.9$ and $C_a = 1.0$. Snapshots are taken at irregular time intervals for illustrative purposes.

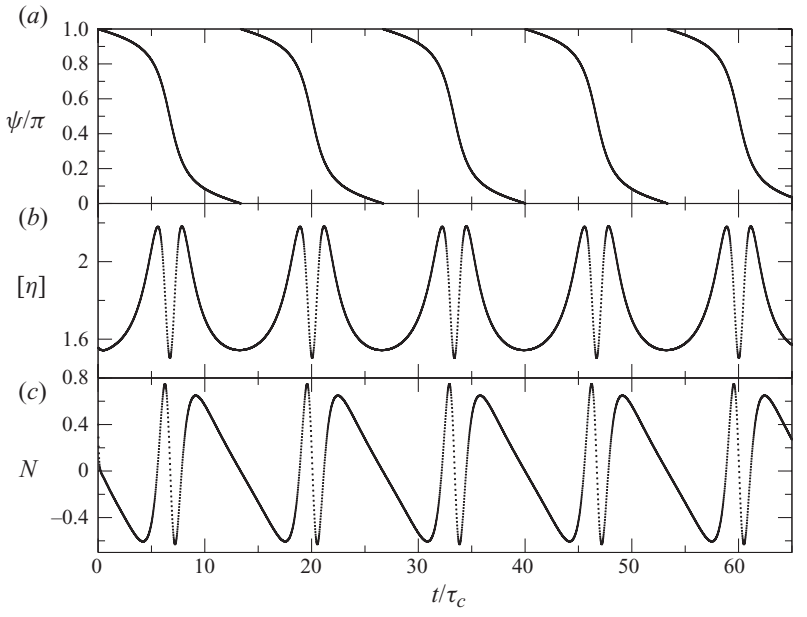

FIGURE 11. Dynamical and rheological quantities in the tumbling regime: (a) inclination angle ψ, (b) reduced viscosity $[\eta]$ and (c) normal stress difference N as a function of time. $\alpha = 0.9$, $\lambda = 8$ and $C_a = 1.0$.

corresponds to the symmetric part of the shear flow) generates dissipation, while the pure rotation corresponds to rigid-body rotations, which do not involve dissipation. The occurrence of two maxima at the orientation $\pm\pi/4$ is due to the maximal strain efficiency in these directions of the dissipative component of the imposed flow on the vesicle. It must be stressed that these maxima are not due to the deformation of the vesicle itself, since they survive even for nearly rigid vesicles ($\lambda = 200$).

The viscosity is minimal when the vesicle aligns with the flow ($\psi = 0$), a somehow trivial effect in the light of the previous discussions. Perhaps, the most astonishing and quite counterintuitive effect is the appearance of a minimum of the viscosity for the vertical position (i.e. $\psi = \pm \pi/2$): our understanding of this result is that the streamlines of the rotational and elongational components of the flow field are parallel to each other (see figure 13), so the competition between the tendency to rotate and strain the vesicle is reduced to a minimum.

The interpretation of the normal stress difference in the periodic regime is at present not completely understood and merits higher attention in the future. Suffice it here to remark (figure 12) that the zeros of the normal stress difference coincide with the extrema of the effective viscosity.

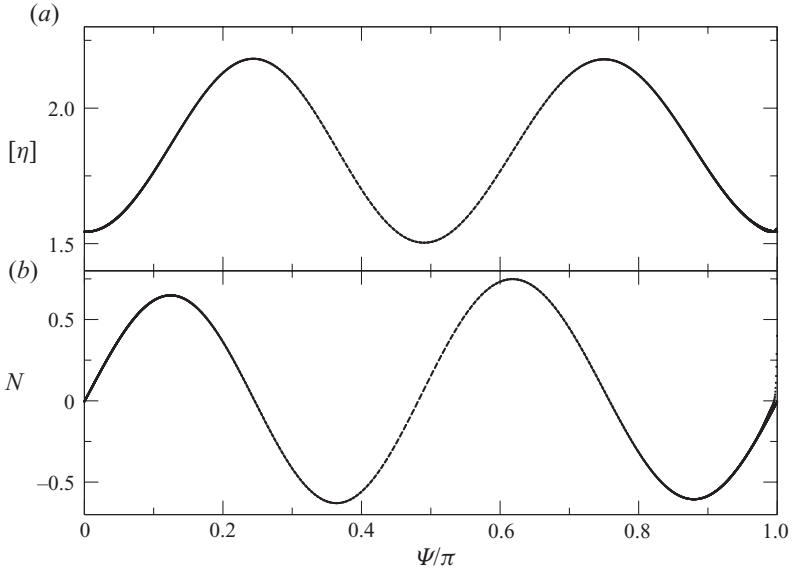

FIGURE 12. Rheological quantities in the tumbling regime: (*a*) reduced viscosity $[\eta]$ and (*b*) normal stress difference N as a function of the instantaneous inclination angle ψ. $\alpha = 0.9$ and $\lambda = 8$. Data are shown between $\psi = 0$ and $\psi = \pi$, in order to stress that the occurrence of two maxima is not related to the obvious symmetry of the rotation of the vesicle by an angle π.

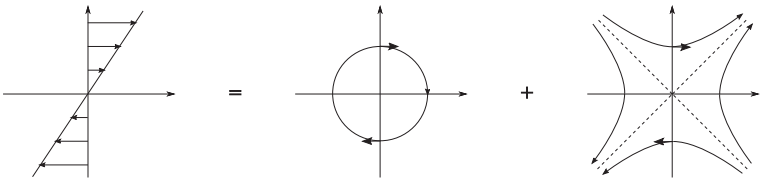

FIGURE 13. Decomposition of the linear shear flow into pure rotational and elongational components.

4.4. *Dependence on shear rate*

We have analysed the behaviour of a vesicle suspension upon increasing the shear rate $\dot{\gamma}$. Two series of simulations have been performed, with capillary numbers $C_a = 1.0$ and $C_a = 10.0$. Vesicles with different reduced areas have been considered: $\alpha \in \{0.70, 0.90, 0.95\}$. The results are reported in figure 6. It can be seen that the sensitivity on the shear rate depends on the reduced area of the vesicle: in the cases $\alpha \in \{0.90, 0.95\}$ there seems to be no significant dependence upon variation of this parameter. Contrariwise, for smaller α, $\alpha = 0.70$, both dynamics and rheology show significant variations because of shear rate (or because of C_a). It is found that upon increasing C_a the transition boundary between tank-treading and tumbling is shifted towards higher values of λ. This effect is traced back to the increase of deformability of the vesicle for significantly deflated vesicles ($\alpha = 0.70$), a fact that is quite invisible for weaker deflation (i.e. for nearly circular shapes), owing to membrane inextensibility (figures 14 and 15). In addition, a decrease in $[\eta]$ is observed in the tumbling regime.

A vesicle suspension can show then a shear thinning behaviour if vesicles are sufficiently deflated. In addition, if their viscosity ratio is close to the critical value λ_c,

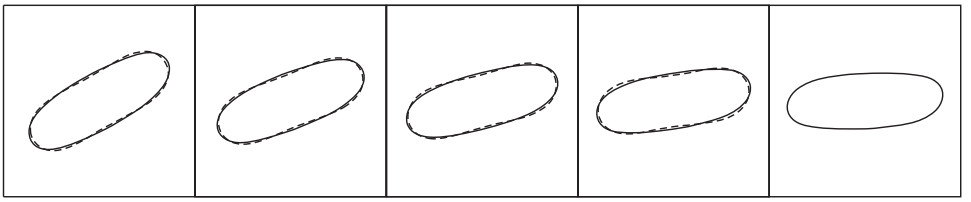

FIGURE 14. Stationary contours of tank-treading vesicles ($\alpha = 0.7$) at $C_a = 10.0$ (solid line) compared with the corresponding ones at $C_a = 1.0$ (dashed line) for different values of the viscosity ratio λ (for $\lambda = 4.0$ and $C_a = 1.0$ there is no tank-treading solution).

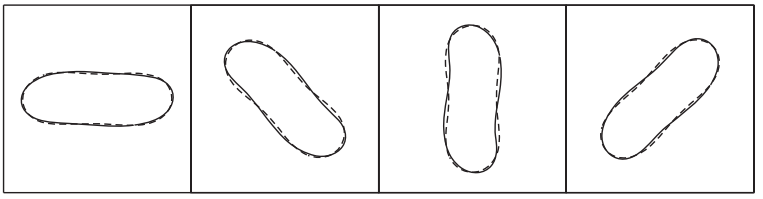

FIGURE 15. Contours of a tumbling vesicle ($\alpha = 0.7$ and $\lambda = 20.0$) at $C_a = 10.0$ (solid line) compared with the corresponding ones at $C_a = 1.0$ (dashed line) for different values of the inclination angle ψ.

a dynamical transition can occur upon variation of the capillary number C_a, affecting even more the effective viscosity: this is shown in figure 16. This complex rheological behaviour (shear thinning triggered by deflation and dynamical transition) contrasts with the case of emulsions, which always show shear thinning (see Kennedy *et al.* 1994; Pal 2000). Drops always deform upon increasing the applied shear but they do not undergo dynamical transitions (except for the possible burst).

Note that the normal stress difference N is normalized in the present paper with the factor $\eta_0\dot{\gamma}$. This contrasts with the conventional notation (used for emulsions, polymer solutions, and so on) $N/\eta_0\dot{\gamma}^2$. It can be checked that the latter is not dimensionless, and its use in literature is dictated by the fact that for a large variety of suspensions of deformable objects $N \sim \dot{\gamma}^2$. In these systems, the quadratic behaviour is due to the presence of an internal (or intrinsic) time scale that depends on $\dot{\gamma}$. This time scale corresponds to the deformation (elongation) of the suspended entities, which is proportional to $\dot{\gamma}$. For vesicles, because of the inextensibility of the membrane, there is a weak dependence of the shape on $\dot{\gamma}$ (see figure 14), and the vesicle elongation quickly attains a saturation regime. Thus, we view the absence of an intrinsic time scale proportional to $\dot{\gamma}$ (see Larson 1999, pp. 418–419), to be the source for the linear behaviour of N with $\dot{\gamma}$ (see also Danker & Misbah 2007 for analytic derivation in the small deformation limit).

4.5. *Comparison with drops*

Since a vesicle is a droplet enclosed in a phospholipidic membrane, a comparison with emulsion rheology will provide valuable information on the role of the membrane. Drops and vesicles are distinctly different systems: (i) drop interface is governed by tension, which resists area increase, while the vesicle membrane is controlled by resistance to bending, and (ii) the drop can change its area, while a vesicle is subject

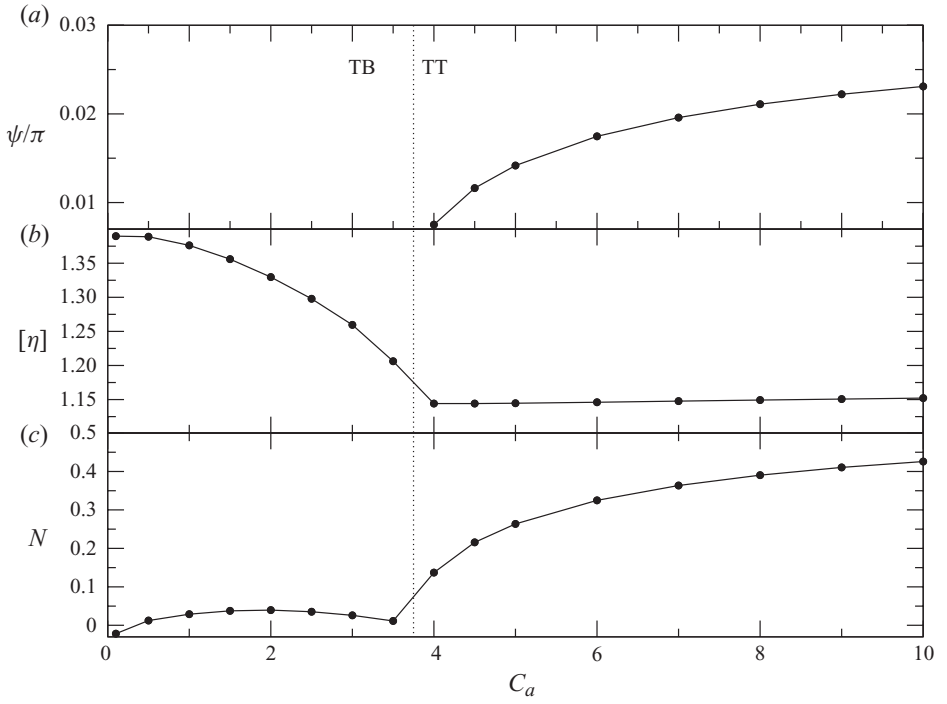

FIGURE 16. Dynamics and rheology of a vesicle with $\alpha = 0.7$, $\lambda = 4.0$ as a function of the capillary number C_a. (*a*) Stationary inclination angle ψ, (*b*) reduced viscosity $[\eta]$ (showing shear thinning) and (*c*) normal stress difference N.

to local membrane inextensibility. The latter property is the most serious ingredient to be emphasized in what follows.

The first difference between vesicle and drop rheology can be obtained by comparing the analytical expressions derived for three-dimensional spherical drops (see Taylor 1932; Frankel & Acrivos 1970) and quasi-spherical vesicles in the tank-treading regime (see Misbah 2006; Danker & Misbah 2007):

$$\frac{\eta}{\eta_0} = 1 + \frac{5}{2}\phi\left(1 - \frac{3}{5(\lambda+1)}\right) \qquad \text{for drops,} \tag{4.2}$$

$$\frac{\eta}{\eta_0} = 1 + \frac{5}{2}\phi\left(1 - \frac{\Delta}{40\pi}(23\lambda + 32)\right) \qquad \text{for vesicles,} \tag{4.3}$$

where Δ, a small parameter in (4.3), is the excess area from a sphere, related to the reduced volume v – the three-dimensional analogue of α – via $\Delta = 4\pi(v^{-2/3} - 1)$. By definition, $v \equiv [V/(4\pi/3)]/[A/(4\pi)]^{3/2}$, where V is the volume and A is the area of the membrane, and $A = r_0^2(4\pi + \Delta)$. While expression (4.2) is an increasing function of λ, i.e. the effective viscosity increases with the internal viscosity of the drop, (4.3) is on the contrary a decreasing function of λ for tank-treading vesicles. This shows that the phospholipid membrane has a significant effect on the rheology of the suspension. Note that (4.2) is obtained by assuming that the drop is spherical. Of course, under shear flow the drop will always deform, but the overall behaviour of the viscosity predicted by Taylor remains essentially the same – provided that the deformation is small enough (see Frankel & Acrivos 1970; Kennedy *et al.* 1994). Therefore, it is reasonable to compare (4.2) with (4.3), which is obtained for a small deformation

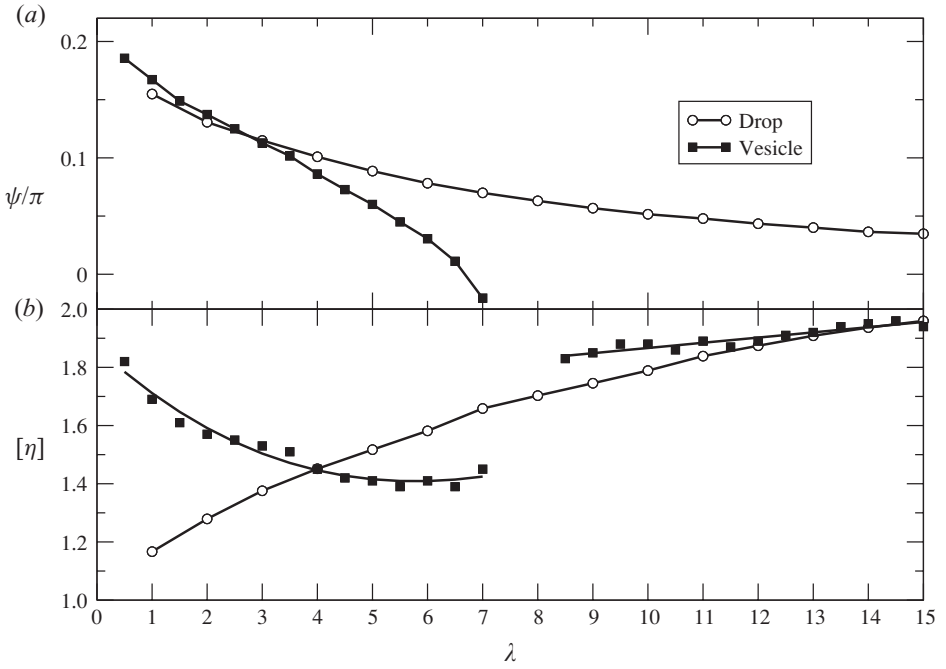

FIGURE 17. Comparison between drop and vesicle suspensions: (*a*) inclination angle ψ in the stationary regimes and (*b*) reduced viscosity $[\eta]$ of a suspension of vesicles (data and guideline) and of a suspension of drops. The data refer to a vesicle of a reduced area $\alpha = 0.9$ and to a drop in a flow having a capillary number $C_{a_\gamma} = 0.3$.

relative to a sphere (for a sphere a vesicle behaves as a rigid particle because of membrane incompressibility).

An exhaustive analysis of drop dynamics and rheology can be found in Kennedy *et al.* (1994), here we shall exploit our own simulations in order to present a clear comparison, focusing on the dependence on the viscosity ratio λ. For this purpose, we have found it more convenient to use the PF model. Indeed, this method delivers directly the velocity field in the whole numerical domain. The analysis of this field will allow us to shed light on the interpretation of the rheological results. Note that the bulk velocity field can be computed within the boundary integral method as well, but this requires some additional numerical treatments.

We define the drop capillary number as $C_{a_\gamma} = \eta_0 \dot{\gamma} R/\gamma$, where γ is the surface tension of the drop, and R is its radius of the equivalent circle. We fix the value of the surface tension of a drop in such a way that the drop shape remains as close as possible to that of the vesicle with reduced area $\alpha = 0.9$ (figure 18). The estimated value of the surface tension that fulfils this requirement yields $C_{a_\gamma} = 0.3$. On the other hand, drops tend to become more circular upon an increase of λ (figure 19). The behaviours of the reduced viscosity as a function of the viscosity ratio λ for a suspension of vesicles and for an emulsion are quite different (figure 17). A comparison of the two behaviours in the range of λ, where both the vesicle and the drop exhibit a stationary shape (i.e. within the tank-treading regime of the vesicles; we consider a low capillary number so that drops maintain their integrity), reveals the same trend difference of (4.2) and (4.3): the reduced viscosity increases for emulsions while it decreases for vesicle suspensions upon increasing λ. A key point in order

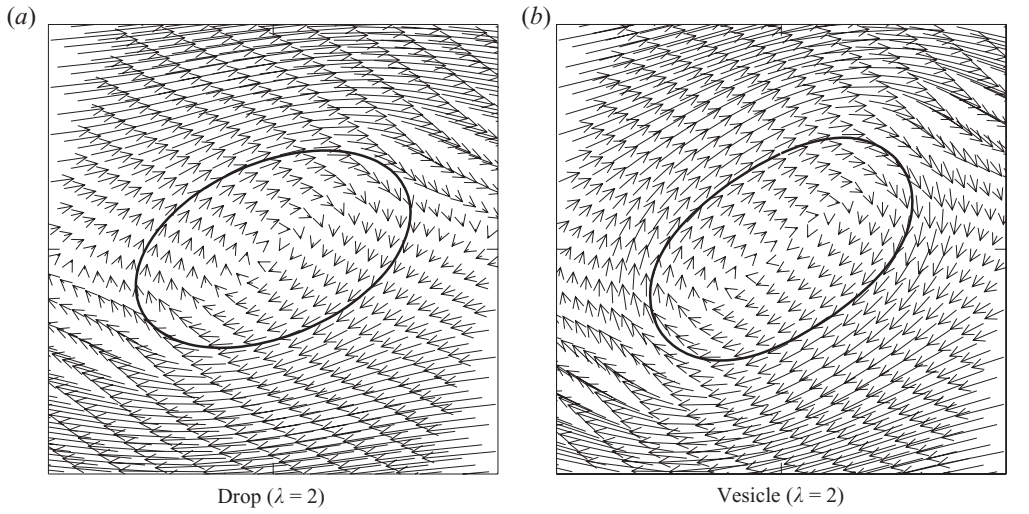

FIGURE 18. A drop (capillary number $C_{a_\gamma} = 0.3$) and a vesicle (reduced surface $\alpha = 0.9$, capillary number $C_a = 1.0$) and their corresponding velocity fields (crop of the central region of the simulation box).

to understand this difference lies in the inspection of the velocity fields around the suspended entities (figure 18).

For a two-dimensional vesicle, the conservation of the local length of the membrane leads to the constraint of uniform velocity around the membrane itself, while the absence of this constraint for drops allows for a non-uniform velocity.

For a vesicle, the perturbation to the velocity field is enhanced further when it occupies a larger section in the direction of the velocity gradient, that is when the orientation angle ψ is large. Since ψ is a decreasing function of λ (figure 17*a*), dissipation is also a decreasing function of λ and consequently the effective viscosity too. This explains the decline of the viscosity in the tank-treading regime; figure 6(*b*). Note also that this effect should be more pronounced for more elongated vesicles (smaller reduced area α), because with the same variation of λ the decline of the tank-treading angle (figure 6*a*) and of the cross-section of the vesicle in the direction of the gradient of the imposed flow (figure 7) are higher. This simple physical interpretation agrees well with the numerical results, which reveal stronger variations of the reduced viscosity for smaller α (figure 6*b*).

The situation with drops is quite different. Note that both the drop and vesicle orientation angles decrease with λ (see figure 17). Nevertheless, in the former case the viscosity increases with λ while the opposite is found in the latter case. A close inspection of both the velocity field and the precise deformation of the drop will be essential to clarify this difference. The viscosity ratio plays a central role and, unlike vesicles (characterised by membrane inextensibility), no constraint is directly imposed on the velocity field by the drop surface. For a drop, increasing internal viscosity means decreasing its deformability. The consequences are twofold: (i) the drop assumes a more circular shape (and thus, unlike vesicles, the cross-section in the direction of the flow gradient does not vary noticeably, as can be seen in figure 19*a*) and (ii) the perturbations caused by a drop on the imposed flow, which are not limited by any surface incompressibility condition, lead to ample enough velocity gradients (and thus to increase of dissipation) close to the surface. This simple argument highlights

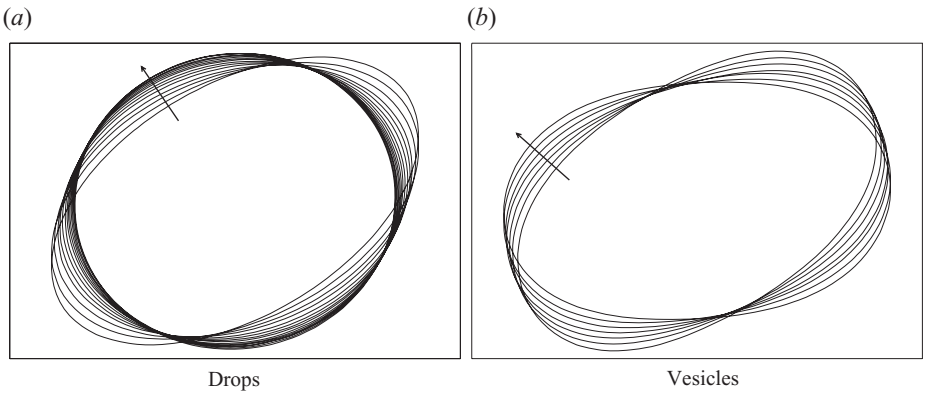

FIGURE 19. Steady contours of (*a*) drops and (*b*) vesicles. For the drops the capillary number is $C_{a_\gamma} = 0.3$ and the viscosity ratio $1 \leqslant \lambda \leqslant 15$ (increasing in the sense of the arrow). For the vesicles the capillary number is $C_a = 1.0$ and the viscosity ratio $1 \leqslant \lambda \leqslant 7$ (increasing in the sense of the arrow). Snapshots are from the PF method.

the central role played by the membrane of the vesicle: not only is the membrane responsible for the various complex dynamics of the vesicle but it also induces a peculiar rheological behaviour. Finally, in the analytical theory to leading order, it is the incompressibility condition for the membrane that controls rheology, and not the bending energy (see Danker & Misbah 2007).

4.6. *Comparison with three-dimensional experiments and theory*

While the present study is focused on two dimensions, it may be worthwhile to attempt a comparison of our results with the available three-dimensional analytical theory and with experiments. Note that before comparing two- and three-dimensional intrinsic viscosities, a preliminary rescaling has to be performed, as dictated by the different values of the Einstein coefficients in two and three dimensions (i.e. we shall attempt the comparison after multiplying two-dimensional data of the intrinsic viscosity by a factor 2.5/2). In addition, we have to convert a reduced volume v (corresponding to three dimensions) into a reduced area α (defined in two dimensions). Since a two-dimensional vesicle corresponds to a translationally invariant form in the direction perpendicular to the shear plane, a natural choice is to consider the maximum section in the shear plane for the three-dimensional vesicle, compute the corresponding reduced area of this section, and then compare it to α.

Once the above preliminary rescaling and conversion are made, we compare the results with those obtained analytically by Danker *et al.* (2007); see figure 20. We focus on the analytical results with $\Delta = 0.25$ (i.e. $v \cong 0.97$ – the value is chosen close to that of a sphere so that the analytical theory is expected to be quantitative), and $C_a = 1.0$. Using the conversion rule discussed above, we find $v = 0.97 \leftrightarrow \alpha = 0.95$. The quantitative agreement between two-dimensional numerical data and three-dimensional analytical results is quite satisfactory. It is interesting to note how the numerical results for $C_a = 1.0$ compare surprisingly well with the analytical ones at $C_a = 10^{-2}$. This can be traced back to the fact that the presence of the VB mode in three dimensions can be suppressed for $C_a = 10^{-2}$ and this has the effect of improving the agreement between two and three dimensions. Note that since for such values of α the results are found to be quite insensitive to C_a (figure 6), taking a smaller value of C_a has as a main effect the suppression of the VB mode and not insignificant alteration of other quantities.

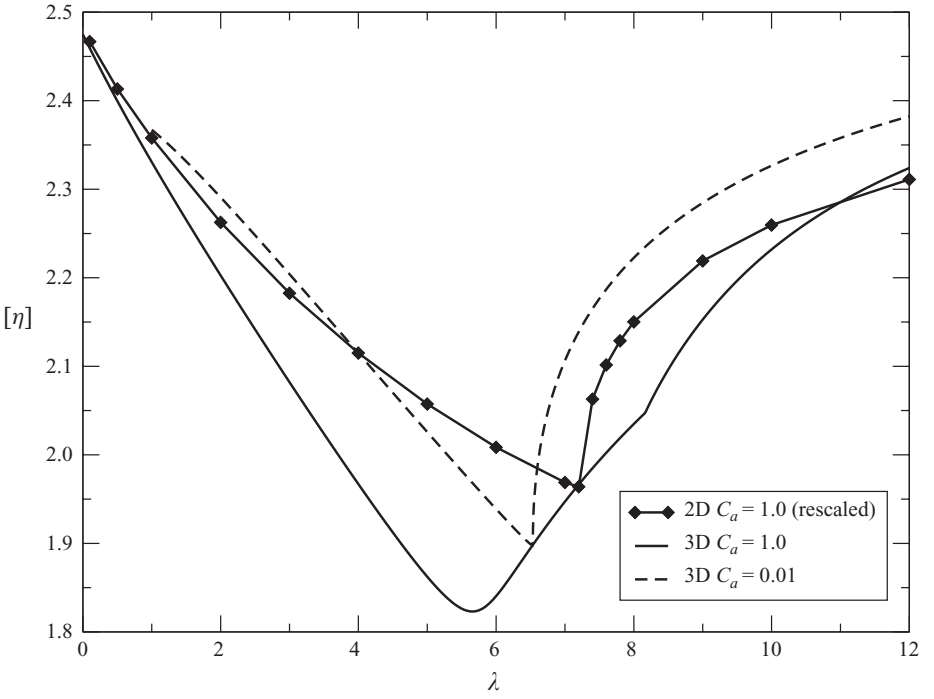

FIGURE 20. Three-dimensional theory ($\Delta = 0.25$) from Danker *et al.* (2007) compared with rescaled two-dimensional results of the present work ($\alpha = 0.95$). Reduced viscosity $[\eta]$ as a function of the viscosity ratio λ.

The comparison with experiments (see Vitkova *et al.* 2008) reported in figure 21 is somehow difficult, due to vesicle polydispersity ($0.9 \leqslant \nu \leqslant 1.0$), and to finite volume concentration ($3\,\% \leqslant \phi \leqslant 12\,\%$) of the samples. If we take $\alpha = 0.90$ we find the corresponding three-dimensional reduced volume to be $\nu = 0.94$ (a value close to the average experimental one). We also rescale our values of the intrinsic viscosity, as explained above. The agreement is partially satisfactory.

5. Conclusion and discussion

We have carried out systematic and quantitative numerical simulations in two dimensions for a dilute suspension of non-interacting vesicles. We have drawn a link between microscopic dynamics and macroscopic rheology, both for the stationary (tank-treading) and for periodic (tumbling) vesicle motions. The central role played by the membrane inextensibility in the rheological behaviour has been clearly demonstrated, and major differences with emulsions have been identified and interpreted. Shear thinning effects have been found and explained in the light of deformation and dynamical transition of the vesicles.

It was not at all obvious at the beginning of this study that the two-dimensional model would capture the main characteristics of the physics, and in particular of the rheology. This is quite encouraging, since it opens the way for extensive calculations for more concentrated suspensions, which are by now quite difficult to handle in three dimensions (due to the large computing time). For example, we are not aware of any three-dimensional numerical simulations based on the BI method that analyses

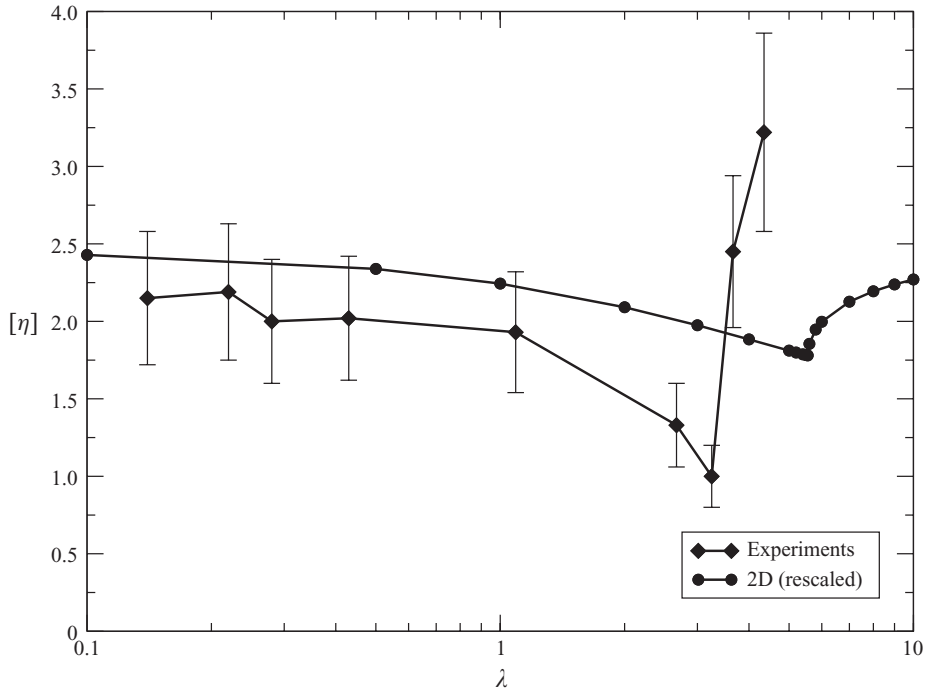

FIGURE 21. Reduced viscosity $[\eta]$ as a function of the viscosity ratio λ. Experimental values from Vitkova *et al.* (2008) are compared with the present work.

quantitatively the full phase diagram (TT, TB and VB) of even a single vesicle under a simple shear flow.

The peculiar behaviour of effective viscosity with the viscosity ratio λ, together with the difference in rheology of emulsions, highlights the non-trivial character of the physics associated with the membrane. Stimulated by recent works on rheology (Misbah 2006; Danker & Misbah 2007), experiments have been carried out by two groups recently (Kantsler *et al.* 2008; Vitkova *et al.* 2008). At low vesicle volume fraction (about 5 %) the results obtained by both groups agree with the prediction of Misbah (2006); Danker & Misbah (2007) and with the present numerical simulation. The agreement is both qualitative and quantitative. At higher volume fraction (> 10 %), the result of Kantsler *et al.* (2008) reports that at small enough λ (about 0.2) the effective viscosity decreases when decreasing λ, in which there should be deviation from theory. The authors attribute this behaviour primarily to hydrodynamic interactions. The experiments of Vitkova *et al.* (2008) performed for the same range of volume fractions did not show the tendency observed by Kantsler *et al.* (2008), a problem that remains a matter for debate. It would be an interesting task for future numerical simulations to show how does the effective viscosity evolve with λ (and with possibly other parameters) when volume fraction is increased. We hope to investigate this matter further in a future paper.

Finally, it must be stressed that red blood cells have often been modelled as elastic capsules (see Eggleton & Popel 1998; Pozrikidis 2003; Bagchi, Johnson & Popel 2005; Lac, Morel & Barthès-Biesel 2007; Mauroy 2008; MacMeccan *et al.* 2009). Some rheological studies have been made regarding the shear thinning effect (see Drochon 2003) of red cells. These studies do not implement local inextensibility

of the membrane, as done here. Red blood cells are inextensible and exhibit shear elastic properties due to cytoskeleton. It is reported in literature (see Evans, Waugh & Melnik 1976) that red blood cells can be stretched up to 5 % before bursting. At a small applied stress the stretching may be due to thermal smoothening of membrane fluctuations (entropic elasticity), and then only when the stress is close to that of cohesive forces that a red cell may reach the rupture threshold. For stresses encountered under ordinary shear rates only entropic elasticity, not included here, may play a role, albeit the precise parameter range when entropy is essential needs to be clarified. We believe that shear elasticity of red cells should be more important than the entropic one, and it would be an interesting task for future work to deal with this question. Nevertheless, it can be stated that if shear elasticity is implemented in the theoretical model of vesicles (see Danker & Misbah 2007), as done for capsules (see Barthès-Biesel & Rallison 1981), then to leading order the effect of membrane shear elasticity scales out of the rheological equations, precisely as does bending rigidity (see Olla 2000). If, on the contrary, the membrane is supposed to have a shear pre-stress, then dynamics and rheology might be affected by membrane elasticity. It will be an interesting task for future investigations to elucidate this question further. This step is essential before making an attempt to compare rheology of vesicle suspension with that of red blood cells.

We are grateful to Alessandro Siria for fruitful discussion and to Alexander Farutin for assistance. We acknowledge financial support from Centre National d'Etudes Spatiales (CNES) and Agence Nationale de la Recherche (ANR MOSICOB).

REFERENCES

Abkarian, M. & Viallat, A. 2008 Vesicles and red blood cells in shear flow. *Soft Matter* **4**, 653–657.

Bagchi, P., Johnson, P. C. & Popel, A. S. 2005 Computational fluid dynamic simulation of aggregation of deformable cells in a shear flow. *J. Biomech. Engng* **127**, 1070–1080.

Barthès-Biesel, D. & Rallison, J. M. 1981 The time-dependent deformation of a capsule freely suspended in a linear shear flow. *J. Fluid Mech.* **113**, 251–267.

Batchelor, G. 1970 The stress system in a suspension of force-free particles. *J. Fluid Mech.* **41** (3), 545–570.

Beaucourt, J., Biben, T. & Misbah, C. 2004*a* Optimal lift force on vesicles near a compressible substrate. *Europhys. Lett.* **67**, 676–682.

Beaucourt, J., Rioual, F., Séon, T., Biben, T. & Misbah, C. 2004*b* Steady to unsteady dynamics of a vesicle in a flow. *Phys. Rev.* E **69**, 011906.

Belzons, M., Blanc, R., Bouillot, J.-L. & Camion, C. 1981 Viscosité d'une suspension diluée et bidimensionnelle de sphères. *C. R. Acad. Sci. Paris* **292**, 5.

Biben, T. 2005 Phase-field models for free-boundary problems. *Eur. J. Phys.* **26**, 47–55.

Biben, T., Kassner, K. & Misbah, C. 2005 Phase-field approach to three-dimensional vesicle dynamics. *Phys. Rev.* E **72**, 041921.

Biben, T. & Misbah, C. 2002 An advected-field method for deformable entities under flow. *Eur. Phys. J.* B **29**, 311–316.

Biben, T. & Misbah, C. 2003 Tumbling of vesicles under shear flow within an advected-field approach. *Phys. Rev.* E **67**, 031908.

Boskovic, S., Chon, J. W. M., Mulvaney, P. & Sader, J. E. 2002 Rheological measurements using microcantilevers. *J. Rheol.* **46** (4), 891–899.

Brady, J. 1984 The Einstein viscosity correction in *n* dimensions. *Intl J. Multiphase Flow* **10**, 113–114.

Canham, P. B. 1970 The minimum energy of bending as a possible explanation of the biconcave shape of the human red blood cell. *J. Theoret. Biol.* **26**, 61–81.

Cantat, I. 1999 Dynamique de vésicules en adhésion. PhD thesis, Université Joseph Fourier, Grenoble.

Cantat, I., Kassner, K. & Misbah, C. 2003 Vesicles in haptotaxis with hydrodynamical dissipation. *Eur. Phys. J.* E **10**, 175–189.

Cantat, I. & Misbah, C. 1999 Dynamics and similarity laws for adhering vesicles in haptotaxis. *Phys. Rev. Lett.* **83** (1), 235–238.

Coupier, G., Kaoui, B., Podgorski, T. & Misbah, C. 2008 Noninertial lateral migration of vesicles in bounded Poiseuille flow. *Phys. Fluids* **20**, 111702.

Danker, G., Biben, T., Podgorski, T., Verdier, C. & Misbah, C. 2007 Dynamics and rheology of a dilute suspension of vesicles: higher-order theory. *Phys. Rev.* E **76**, 041905.

Danker, G. & Misbah, C. 2007 Rheology of a dilute suspension of vesicles. *Phys. Rev. Lett.* **98**, 088104.

Danker, G., Verdier, C. & Misbah, C. 2008 Rheology and dynamics of vesicle suspension in comparison with droplet emulsion. *J. Non Newton. Fluid Mech.* **152** (1–3), 156–167 (Fourth International workshop on Nonequilibrium Theromdynamics and Complex Fluids).

Danker, G., Vlahovska, P. M. & Misbah, C. 2009 Vesicles in Poiseuille flow. *Phys. Rev. Lett.* **102** (14), 148102.

Deschamps, J., Kantsler, V. & Steinberg, V. 2009 Phase diagram of single vesicle dynamical states in shear flow. *Phys. Rev. Lett.* **102** (11), 118105.

Drochon, A. 2003 Rheology of dilute suspensions of red blood cells: experimental and theoretical approaches. *Eur. Phys. J. AP* **22** (2), 155–162.

Edidin, M. 2003 Lipids on the frontier: a century of cell-membranes bilayer. *Nature* **4**, 414–418.

Eggleton, C. D. & Popel, A. S. 1998 Large deformation of red blood cell ghosts in a simple shear flow. *Phys. Fluids* **10**, 1834–1845.

Einstein, A. 1906 Eine neue Bestimmung der Moleküldimensionen. *Ann. Phys.* **19**, 289–306.

Einstein, A. 1911 Berichtigung zu meiner Arbeit: Eine neue Bestimmung der Moleküldimensionen. *Ann. Phys.* **34**, 591–592.

Evans, E. A., Waugh, R. & Melnik, L. 1976 Elastic area compressibility modulus of red cell membrane. *Biophys. J.* **16**, 585–595.

Finken, R., Lamura, A., Seifert, U. & Gompper, G. 2008 Two-dimensional fluctuating vesicles in linear shear flow. *Eur. Phys. J.* E **25**, 309–321.

Folch, R., Casademunt, J., Hernández-Machado, A. & Ramíirez-Piscina, L. 1999 Phase-field model for Hele-Shaw flows with arbitrary viscosity contrast. Part 1. Theoretical approach. *Phys. Rev.* E **60**, 1724–1733.

Frankel, N. A. & Acrivos, A. 1970 The constitutive equation for a dilute emulsion. *J. Fluid Mech.* **44** (1), 65–78.

Helfrich, W. 1973 Elastic properties of lipid bilayers: theory and possible experiments. *Z. Naturforsch.* **28**, 693–703.

Hohenberg, P. & Halperin, B. 1977 Theory of dynamic critical phenomena. *Rev. Mod. Phys.* **49**, 435–479.

Jamet, D. & Misbah, C. 2007 Towards a thermodynamically consistent picture of the phase-field model of vesicles: local membrane incompressibility. *Phys. Rev.* E **76**, 051907.

Jamet, D. & Misbah, C. 2008*a* Thermodynamically consistent picture of the phase-field model of vesicles: elimination of the surface tension. *Phys. Rev.* E **78**, 041903.

Jamet, D. & Misbah, C. 2008*b* Toward a thermodynamically consistent picture of the phase-field model of vesicles: curvature energy. *Phys. Rev.* E **78**, 031902.

Kantsler, V., Segre, E. & Steinberg, V. 2008 Dynamics of interacting vesicles and rheology of vesicle suspension in shear flow. *Europhys. Lett.* **82** (5), 58005.

Kantsler, V. & Steinberg, V. 2005 Orientation and dynamics of a vesicle in tank-treading motion in shear flow. *Phys. Rev. Lett.* **95**, 258101.

Kantsler, V. & Steinberg, V. 2006 Transition to tumbling and two regimes of tumbling motion of a vesicle in shear flow. *Phys. Rev. Lett.* **96**, 036001.

Kaoui, B., Biros, G. & Misbah, C. 2009 Why do red blood cells have asymmetric shapes even in a symmetric flow? *Phys. Rev. Lett.* **103**, 188101.

Kaoui, B., Ristow, G., Cantat, I., Misbah, C. & Zimmermann, W. 2008 Lateral migration of a 2D vesicle in unbounded Poiseuille flow. *Phys. Rev.* E **77**, 021903.

Keller, S. & Skalak, R. 1982 Motion of a tank-treading ellipsoidal particle in a shear flow. *J. Fluid Mech.* **120**, 27–47.

Kennedy, M. R., Pozrikidis, C. & Skalak, R. 1994 Motion and deformation of liquid drops, and rheology of dilute emulsions in simple shear flow. *Comput. Fluids* **23** (2), 251–278.

Kobayashi, R. 1993 Modeling and numerical simulations of dendritic crystal growth. *Physica* D **63**, 410–423.

Kraus, M., Wintz, W., Seifert, U. & Lipowsky, R. 1996 Fluid vesicles in shear flow. *Phys. Rev. Lett.* **77**, 3685–3688.

Lac, E., Morel, A. & Barthès-Biesel, D. 2007 Hydrodynamic interaction between two identical capsules in simple shear flow. *J. Fluid Mech.* **573**, 149–169.

Larson, R. G. 1999 *The Structure and Rheology of Complex Fluids*. Oxford University Press.

Lebedev, V. V., Turitsyn, K. S. & Vergeles, S. S. 2008 Nearly spherical vesicles in an external flow. *New J. Phys.* **10** (4), 043044.

MacMeccan, R. M., Clausen, J. R., Neitzel, G. P. & Aidun, C. K. 2009 Simulating deformable particle suspensions using a coupled lattice-Boltzmann and finite-element method. *J. Fluid Mech.* **618**, 13–39.

Mader, M.-A., Vitkova, V., Abkarian, M., Viallat, A. & Podgorski, T. 2006 Dynamics of viscous vesicles in shear flow. *Eur. Phys. J.* E **19**, 389–397.

Maitre, E., Milcent, T., Cottet, G.-H., Raoult, A. & Usson, Y. 2009 Applications of level set methods in computational biophysics. *Math. Comput. Model.* **49**, 2161–2169.

Mauroy, B. 2008 Following red blood cells in a pulmonary capillary. *ESAIM Proc.* **23**, 48–65.

McWhirter, J. L., Noguchi, H. & Gompper, G. 2009 Flow-induced clustering and alignment of vesicles and red blood cells in microcapillaries. *Proc. Natl Acad. Sci. USA* **106**, 6039–6043.

Messlinger, S., Schmidt, B., Noguchi, H. & Gompper, G. 2009 Dynamical regimes and hydrodynamic lift of viscous vesicles under shear. *Phys. Rev.* E **80** (1), 011901.

Misbah, C. 2006 Vacillating breathing and tumbling of vesicles under shear flow. *Phys. Rev. Lett.* **96**, 028104.

Noguchi, H. & Gompper, G. 2005 Shape transitions of fluid vesicles and red blood cells in capillary flows. *Proc. Natl Acad. Sci. USA* **102**, 14159–14164.

Olla, P. 2000 The behaviour of closed inextensible membranes in linear and quadratic shear flows. *Physica* A **278**, 87–106.

Pal, R. 2000 Shear viscosity behaviour of emulsions of two immiscible liquids. *J. Colloid Interface Sci.* **225**, 359–366.

Penrose, O. & Fife, P. 1990 Thermodynamically consistent models of phase-field type for the kinetics of phase transitions. *Physica* D **43**, 44–62.

Pozrikidis, C. 1992 *Boundary Integral and Singularity Methods for Linearized Viscous Flow*. Cambridge University Press.

Pozrikidis, C. 1993 On the transient motion of ordered suspensions of liquid drops. *J. Fluid Mech.* **246**, 301–320.

Pozrikidis, C. 2001 Interfacial dynamics for stokes flow. *J. Comput. Phys.* **169**, 250–301.

Pozrikidis, C. 2003 Numerical simulation of the flow-induced deformation of red blood cells. *Ann. Biomed. Engng* **31**, 1194–1205.

Rallison, J. M. & Acrivos, A. 1978 A numerical study of the deformation and burst of a viscous drop in an extensional flow. *J. Fluid Mech.* **89** (1), 191–200.

Rioual, F., Biben, T. & Misbah, C. 2004 Analytical analysis of a vesicle tumbling under a shear flow. *Phys. Rev.* E **69**, 061914.

Schowalter, W. R., Chaffey, C. E. & Brenner, H. 1968 Rheological behaviour of a dilute emulsion. *J. Colloid Interface Sci.* **26**, 152–160.

Taylor, G. 1932 The viscosity of a fluid containing small drops of another fluid. *Proc. R. Soc. Lond.* A **138**, 41–48.

Veerapaneni, S. K., Gueyffier, D., Zorin, D. & Biros, G. 2009 A boundary integral method for simulating the dynamics of inextensible vesicles suspended in a viscous fluid in 2D. *J. Comput. Phys.* **228**, 2334–2353.

Vitkova, V., Mader, M.-A., Polack, B., Misbah, C. & Podgorski, T. 2008 Micro–macro link in rheology of erythrocyte and vesicle suspensions. *Biophys. J.* **95**, 33–35.

Vlahovska, P. M. & Gracia, R. S. 2007 Dynamics of a viscous vesicle in linear flows. *Phys. Rev.* E **75** (1), 016313.

van der Waals, J. 1979 The thermodynamic theory of capillarity under the hypothesis of a continuous variation of density. *J. Stat. Phys.* **20**, 200–244.

Wang, S., Sekerka, R., Wheeler, A., Murray, B., Coriell, S. R., Braun, R. J. & McFadden, G. B. 1993 Thermodynamically-consistent phase-field models for solidification. *Physica* D **69**, 189–200.

Wheeler, A., Boettinger, W. & McFadden, G. 1993 Phase-field model of solute trapping during solidification. *Phys. Rev.* E **47**, 1893–1909.

Willenbacher, N. & Oelschlaeger, C. 2007 Dynamics and structure of complex fluids from high frequency mechanical and optical rheometry. *Curr. Opin. Colloid Interface Sci.* **12** (1), 43–49.